PHYSICAL REVIEW B VOLUME 25, NUMBER 4 15 FEBRUARY 1982

Macroscopic theory of pulsed-laser annealing. III. Nonequilibrium segregation effects

R. F. Wood

Solid State Division of Oak Ridge National Laboratory, Oak Ridge, Tennessee 37830

(Received 29 June 1981)

During the past three years, phenomena associated with pulsed and cw laser annealing of semiconductors have generated intense interest among scientists in both fundamental and applied areas of solid-state physics and materials science. As a consequence, a coherent picture of the physical processes involved, at least on a macroscopic basis, is beginning to emerge. In the first two papers of this series, the results of heat and mass (dopant) transport calculations based on the melting model of pulsed-laser annealing were described in considerable detail. It was shown that dopant profiles observed after pulsed-laser annealing could not be fitted when values of the interface segregation coefficient k_i^0 appropriate for solidification under nearly thermodynamic equilibrium conditions were used in the dopant redistribution calculations. In this paper, a model is developed which relates the nonequilibrium interface segregation coefficient k_i to k_i^0 and to the velocity of the liquid-solid interface during recrystallization of the molten region created by the laser radiation. The functional dependence of k_i on the interface velocity cannot be calculated exactly, but simple approximate expressions for this dependence yield results which are in accord with the experimental data presently available. Moreover, with the use of the velocity dependence of k_i, it is shown that the model gives satisfactory agreement with the maximum nonequilibrium dopant concentrations which have been observed for an interface velocity of ~ 4 m/sec. It is further shown that when the velocity-dependent k_i is used in the theory of Mullins and Sekerka for cellular formation during solidification, agreement with the results of pulsed-laser annealing experiments is obtained, but if k_i^0 is used there is no agreement. The relationship of the model to the general concept of "solute trapping" introduced by Baker and Cahn is discussed and it is shown that the model satisfies the criterion for solute trapping.

I. INTRODUCTION

This is the third in a series of papers on the melting model of pulsed-laser annealing. In paper I,[1] the physical models and finite difference techniques used in the heat transport and melting calculations were explained and extensive results of the calculations were given. In paper II,[2] the results of paper I were used to obtain theoretical dopant profiles in Si after irradiation with pulses from a Q-switched ruby laser and these were compared to profiles measured primarily by secondary ion mass spectroscopy (SIMS), and Rutherford backscattering (RBS). Segregation effects were included in the calculations, but the interface segregation coefficient k_i was taken as an adjustable parameter. The values of k_i needed to fit the experimental dopant profiles were greatly different from reported values of the equilibrium segregation coefficient k_i^0, which is appropriate for crystal growth under conditions closely approaching thermodynamic equilibrium. In this paper, a model[3] which relates k_i to k_i^0 is developed in detail. The model is based on kinetic rate equations and introduces an activation energy for dopant transitions from the solid to the liquid which is a function of the velocity of the liquid-solid interface. The functional form of this activation energy cannot be determined completely, but its limiting behavior can be defined. Simple approximate forms for the velocity-dependent activation energy allow k_i as a function of k_i^0 and the interface velocity to be determined. The velocity-dependent k_i is then used in well-developed theories to explain several nonequilibrium segregation effects which have been observed during pulsed-laser annealing.

The paper is divided into seven sections. In Sec. II a brief survey of the experimental evidence for

the occurrence of nonequilibrium thermodynamic processes during pulsed-laser annealing is given. The kinetic rate model for nonequilibrium segregation, originally given in Ref. 3, is further developed in Sec. III, and in Sec. IV the implications of the model for the question of solubility limits as a function of laser annealing conditions are explored. In Sec. V, it is shown that the Mullins and Sekerka[4] theory of cellular formation during solidification provides a satisfactory description of the observed data for nonuniform segregation of various dopants in silicon if the velocity-dependent interface segregation coefficients are used. In Sec. VI, additional discussion of various aspects of the calculations and experiments are given and it is shown that the model satisfies the criterion for "solute trapping." A brief review of other attempts to develop a theory of nonequilibrium segregation is also given in this section. Finally, the contents of the three papers in this series are summarized and some concluding remarks are made about the importance of the laser-annealing phenomenon for the development of our understanding of ultrarapid crystallization and related areas of materials science and solid-state physics.

II. EXPERIMENTAL EVIDENCE FOR NONEQUILIBRIUM SEGREGATION EFFECTS

In one of the earliest papers on laser annealing of ion-implanted Si, Khaibullin *et al.*[5] reported that the concentration of dopants after annealing could exceed conventional solid solubility limits. It was recognized that this result implied that nonequilibrium thermodynamic processes occur during laser annealing. Early calculations[6,7] of the penetration and velocity v of the liquid-solid interface or melt front during pulsed-laser annealing showed that the near-surface regions of the samples melt and recrystallize in times of the order of 100 nsec and that during recrystallization v is of the order of a few m/sec; these and other results were discussed thoroughly in papers I and II of this series. Nonequilibrium segregation effects during rapid recrystallization have been considered in the literature,[8,9] but until the discovery of laser annealing the range of crystallization velocities attainable under well-controlled experimental conditions was too small to test various proposed models, most of which can now be shown to be inadequate or incomplete.

Values[10] of the equilibrium interface segregation coefficient k_i^0 for B, P, and As in Si are 0.80, 0.35, and 0.3, respectively. Standard theories of solidification based on diffusion equations,[11] when applied to the laser-annealing process, show that in As- and P-implanted Si these values of k_i^0 should produce large concentration spikes at the surface which would be easily observable by a variety of techniques such as secondary ion mass spectroscopy and Rutherford backscattering. These surface spikes are not observed in B-, As-, and P-implanted laser-annealed Si,[12] nor in As-doped amorphous Si layers recrystallized by a laser.[13] Moreover, satisfactory fits to the dopant profiles in these cases can only be obtained with values of k_i nearly equal to unity.[6,12,13] The fact that equilibrium solubility limits can be exceeded in systems such as these, which have retrograde solubility, can be taken as further evidence for nonequilibrium growth processes.[5,8,9,14,15] Although the question of how and to what extent equilibrium solubility limits can be exceeded during pulsed-laser annealing is one of the most fascinating aspects of the process, in the author's opinion the absence of segregation peaks for certain dopants at concentrations well below the solubility limit is of more fundamental importance for understanding the basic mechanisms of ultrarapid crystallization.

Recently White *et al.*[15] used RBS techniques to measure the profiles of Ga, In, and Bi in ion-implanted, laser-annealed Si. The results, together with earlier data on Sb and As, were analyzed using a model of dopant diffusion which included segregation effects and utilized melt-front information supplied by the present author from calculations such as those in Ref. 1; from fits of the measured profiles values of k_i were extracted. Similar, but somewhat more rigorous calculations, were carried out in paper II of this series. The results of White *et al.* and of Refs. 2, 6, 12, and 13 provide data on the segregation behavior of B, P, As, Sb, Ga, In, and Bi, in Si during laser annealing. Values of k_i^0 from the compilation of Trumbore[10] and of k_i from Refs. 2 and 15 are shown in Table I. The most striking feature of these data is the very large differences between k_i^0 and k_i, especially when k_i^0 is small. Table I also shows the approximate ratios of the nonequilibrium dopant concentrations C_d^s to the maximum equilibrium concentrations C_d^{so} reported in Ref. 15. The remarkable extent to which the equilibrium solubility limits can be exceeded is evident. The values of D_l, the dopant diffusion coefficient in liquid Si shown

TABLE I. Experimental data. Values of k_i are not directly measurable; they can be determined only by theoretically fitting experimental dopant profiles.

Dopant	k_i^0	k_i (Ref. 14)	k_i (Ref. 2)	C_d^s/C_d^{so} (Ref. 14)	D_l (Ref. 24) 10^4 cm^2/sec	D_l (Ref. 22) 10^4 cm^2/sec
B	0.8		~1.0		2.4±0.7	3.3 ±0.4
P	0.35		~1.0		5.1±1.7	2.7 ±0.3
As	0.3	1.00	~1.0	4	3.3±0.9	
Sb	0.023	0.7	0.8 −1.0	18	1.5±0.5	1.4 ±0.5
Ga	0.008	0.2	0.15−0.3	10	4.8±1.5	0.66±0.5
In	0.0004	0.15	0.10−0.20	188	6.9±1.2	0.17±0.3
Bi	0.0007	0.4	0.25−0.35	500		

Table I, will be used later.

At least two groups[16] have reported cellular structure in the distribution of impurities in Si samples coated with thin metallic films and irradiated with Q-switched lasers. More recently, a number of groups[17] have observed similar structures in ion-implanted, laser-annealed Si samples. Cellular structure is characteristic of solidification processes in which for one reason or another the planar liquid-solid interface becomes unstable during crystallization. In a two-component system, the cells themselves consist primarily of one component while the second component is segregated to the cell walls. Experimental data on laser-annealed silicon samples is not yet extensive enough to give a complete picture of the cellular formation process; however, the data that are available clearly indicate that the dopant concentrations at the onset of cellular formation during pulsed-laser annealing greatly exceed those found in growth near equilibrium.[18]

III. KINETIC MODEL OF NONEQUILIBRIUM SOLIDIFICATION

A. Rate equations and the segregation coefficient

Rate equations[19] for the incorporation of host h and dopant d atoms into the solid can be written as

$$R_j = K_j^f c_j^l - K_j^r C_j^s, \quad j = h,d \ . \tag{1}$$

C_j^l and C_j^s are the concentrations (in atomic fractions) of j-type atoms in the liquid and solid at the interface, and K_j^f and K_j^r are the forward (liquid $\rightarrow$ solid) and reverse rate constants in m/sec. In general, the rate constants will depend on conditions (e.g., phases, temperature, etc.) in both the liquid and the solid. For the present, it will be assumed that the dopant atoms are in a dispersed phase in both liquid and solid, although this assumption is not strictly necessary for the development in this subsection. In the absence of any significant diffusion in the solid, the rate at which the concentration of h and d appear in the solid is just the growth velocity v times the concentration observed in the solid, or $R_j = vC_j^s$. Adding Eqs. (1) and noting that

$$C_h^l + C_d^l = C_h^s + C_d^s = 1 \tag{2}$$

gives

$$v = K_h^f c_h^l + K_d^f C_d^l - K_h^r C_h^s - K_d^r C_d^s \tag{3}$$

and, for $j = d$,

$$vC_d^s = K_d^f C_d^l - K_d^r C_d^s \ . \tag{4}$$

The explicit dependence of Eqs. (3) and (4) on v can be eliminated to obtain [again using Eq. (2)]

$$K_h^f C_h^l C_d^s + K_d^f C_d^l C_d^s - (K_h^r - K_d^r) C_h^s C_d^s = K_d^f C_d^l \ . \tag{5}$$

Let us assume that the dopant concentration in the solid does not exceed ~5−10 %, put $C_h^s = 1 - C_d^s$ in the third term on the left-hand side of Eq. (5), neglect terms in $(C_d^s)^2$, and thus obtain the equation

$$(K_h^f C_h^l + K_d^f C_d^l) C_d^s - (K_h^r - K_d^r) C_d^s = K_d^f C_d^l \ . \tag{6}$$

The interface segregation coefficient for the dopant is defined by

$$k_i \equiv C_d^s / C_d^l \ . \tag{7a}$$

It should be noted that at this point this definition does not involve a phase diagram or any related thermodynamic considerations, and therefore it does not specify the phases that are present in either the solid or liquid. It follows directly from Eq. (6) that

$$k_i = K_d^f [(K_h^f - K_d^f) C_h^l + K_d^f - K_h^r + K_d^r]^{-1} \ , \tag{7b}$$

or

$$k_i = \frac{K_d^f}{K_d^r} \left[1 + \frac{K_d^f - K_h^r}{K_d^r} + \frac{K_h^f - K_d^f}{K_d^r} C_h^l \right]^{-1} \ . \tag{7c}$$

An alternative expression for k_i, obtained by setting $C_h^l = 1 - C_d^l$, is

$$k_i = \frac{K_d^f}{K_d^r} \left[1 + \frac{K_h^f - K_h^r}{K_d^r} - \frac{K_h^f - K_d^f}{K_d^r} C_d^l \right]^{-1} \ . \tag{7d}$$

It will be shown below that the expression in the parentheses of Eqs. (7c) and (d) are nearly unity for most cases of interest here. However, it is useful first to consider the expression for k_i which comes from Eq. (4) above i.e.,

$$k_i = K_d^f (v + K_d^r) = \frac{K_d^f}{K_d^r} \left[1 + \frac{v}{K_d^r} \right]^{-1} \ . \tag{8}$$

If K_d^f and K_d^r are assumed not to depend on v, then k_i will decrease as v increases, which is completely contrary to the experimental data. In Eq. (7d), on the other hand, the *explicit* dependence of k_i on v has been eliminated and if it were again assumed that the K's are independent of v, the only dependence on the interface velocity would have to come through C_d^l (this is not quite true, as will be discussed below). Of course, C_d^l does depend on v (Ref. 11), but if this were the dependence of importance here Eq. (7d) would predict that k_i would attain its maximum value only when $C_d^l = 1$. It is highly unlikely that the case $C_d^l = 1$ could occur for a binary system since it would mean that $C_h^l = 0$.

It is useful to note that for a pure material ($C_d^l = C_d^s = 0$), Eq. (3) gives

$$v = K_h^f - K_h^r \ . \tag{9}$$

Chalmers[20] has estimated that rate constants encountered in equilibrium freezing are of the order of 100 m/sec; hence, the K's are expected to be much larger than v. For dopant atoms in Si which maintain the same bonding characteristics existing between the Si atoms themselves (e.g., III, IV dopants), the forward rate constants should be roughly related to the diffusion coefficients in the liquid D_l.[20] From Table I, it can be seen that values of D_l do not vary greatly for group III and V dopants in Si. Furthermore, because D_l is not likely to be significantly affected by the crystallization velocity, it should be a good approximation to put

$$K_d^f = K_h^f = K_d^{fo} = K_h^{fo} \ . \tag{10}$$

This approximation may be questionable for dopants such as Fe, Co, Ag, Au, etc. whose bonding properties in Si differ greatly from those of group III and V dopants, but the equalities expressed in Eq. (10) will be used throughout this paper.

Turning now to the consideration of the terms in the parentheses in Eq. (7d), it is seen that the second term is the difference between two nearly equal large quantities divided by a large quantity and must therefore be small. Using Eq. (9), this term can be written to a good approximation as v/K_d^r which, as we have seen in Eq. (8), gives the wrong velocity-dependence to k_i. Since C_d^l cannot exceed 1 (and, in fact, is expected to be much less than 1), the third term is also small, and tends to cancel the second term. Therefore, it can be concluded that for dilute solutions and for $v << K_d^r$, k_i is given to a quite good approximation by the simple form

$$k_i = K_d^f / K_d^r \ . \tag{11}$$

Since there is no explicit dependence of k_i on v in this equation, we are forced to the conclusion that the velocity dependence must come in through the rate "constants" themselves. Let us consider next how the rate constants can be expressed in terms of velocity-dependent activation energies.

B. Velocity-dependent activation energies

It was noted above that forward rate constants are not expected to depend strongly on the dopant since diffusion coefficients in the liquid do not vary greatly (i.e., by orders of magnitude, as in the solid) with dopant. It will be assumed now that all of the rate constants are of the activated form, e.g.,

$$K_d^r = A_d^r \exp(-U_d^r/kT) , \tag{12}$$

in which U_d^r is the effective barrier height against jumps of a dopant atom from the solid into the liquid. The coefficient A_d^r is a product of a geometrical and a frequency factor, an "accommodation coefficient," and possibly other factors.[19] It seems reasonable that none of these factors will depend strongly on v, and hence it will be assumed that $A_j^f = A_j^{f0}$ and $A_j^r = A_j^{r0}$ for $j = h$ and d. To account for dopant trapping, U_d^r is written as

$$U_d^r(v) = U_d^{r0} + \Delta U_d^r(v) , \tag{13}$$

where U_d^{r0} is the "equilibrium" ($v = 0$) value of the activation energy. $\Delta U_d^r(v)$ may be a complicated function of v, but it must go to 0 as $v \to 0$ and to an asymptotic value as v becomes large; simple analytic forms for it will be discussed shortly. It should be understood that only U_d^r is being assigned a velocity dependence; all other U's remain constant. Introduction of the factor $F \equiv A_d^r / A_d^{r0}$ and use of Eq. (13) allows Eq. (12) to be written as

$$K_d^r = F A_d^{r0} \exp(-U_d^{r0}/kT) \exp[-\Delta U_d^r(v)/kT]$$

$$= F K_d^{r0} \exp[-\Delta U_d^r(v)/kT] . \tag{14}$$

Using Eq. (14) and $K_d^f = K_d^{f0}$ from Eq. (10) in Eq. (11) then gives

$$k_i = (K_d^{f0}/F K_d^{r0}) \exp[\Delta U_d^r(v)/kT]$$

$$= (k_i^0/F) \exp[\Delta U_d^r(v)/kT] , \tag{15}$$

where $k_i^0 \equiv K_d^{f0}/K_d^{r0}$ is the equilibrium interface segregation coefficient. Note that the condition imposed on the A factors just before Eq. (13) requires that $F = 1$. Next let us write

$$\Delta U_d^r(v) = \Delta U_d^{ra} f(v) , \tag{16}$$

where $f(v)$ is a function that goes to 0 as $v \to 0$ and to 1 as $v \to \infty$, and ΔU_d^{ra} is the asymptotic value of $\Delta U_d^r(v)$ as v becomes very large. It should be noted that v can never exceed K_h^f (the so-called "sticking" limit), but for convenience the notation $v \to \infty$ will be used frequently. If it is required that $k_i \to 1$ as $v \to \infty$, then it is easily shown that

$$\Delta U_d^{ra} = -kT \ln k_i^0 . \tag{17}$$

The value of T can be fixed by noting that ΔU_d^{ra} is obtained when $v \to \infty$. Assuming that the liquid is not significantly supercooled, the velocity will have its maximum possible value when the temperature of the liquid is at the melting point and the solid just on the other side of the interface is at the lowest possible value ($T = 0\,\mathrm{K}$). It follows that T can be taken as the melting temperature, which for a dilute solution is very nearly that for the pure host material, i.e., T_h. Because of the assumption about the A's, F in Eq. (15) is constrained to be unity and hence

$$k_i = k_i^0 \exp[(-kT_h \ln k_i^0) f(v)/kT] . \tag{18}$$

It is interesting to note that the condition $F = 1$ follows not only from the requirements on the A factors ($A_d^r = A_d^{r0}$), but also from the limiting behavior of k_i (at small v) as long as the A factors are independent of v. However, it would be possible to make A_d^r and hence F a function of v such that $F \to 1$ as $v \to 0$ and to some constant value as $k_i \to 1$; this would involve a redefinition of ΔU_d^{ra} and make it velocity dependent. It would also be possible to let k_i go to some maximum value of k_i other than 1 as $v \to \infty$, but this would also involve a redefinition of ΔU_d^{ra}. These seem unwarranted complications at this stage in the development of the model.

Approximate forms for $\Delta U_d^r(v)$ can be justified on the basis of the physical process illustrated schematically in Fig. 1. Assume that during steady-state recrystallization the material in the vicinity of the advancing melt front can be divided into three regions. In regions S and L, the material has the properties of the solid and liquid, respectively. In the interface region I between S and L, the properties change in some continuous fashion between those of regions S and L. At time $t = 0$, a dopant atom is deposited at the beginning of I. As solidification proceeds and the interface region moves across the original position of the deposited atom, a time-dependent, effective, one-dimensional potential barrier $U_d^r(v,t)$ against escape back into the liquid is created because of the addition of layers of host atoms. This effective barrier arises from a series of potential wells in region I between which the dopant atom hops. The exact form of $U_d^r(v,t)$ would be extremely difficult to calculate, even if the deposited atom remained fixed while region I moves. A molecular dynamics calculation, e.g., might give some insight into $U_d^r(v,t)$ under this condition. However, while region I is moving across the original position of the deposited atom, the atom itself will tend to diffuse toward the L region and this further complicates the problem.

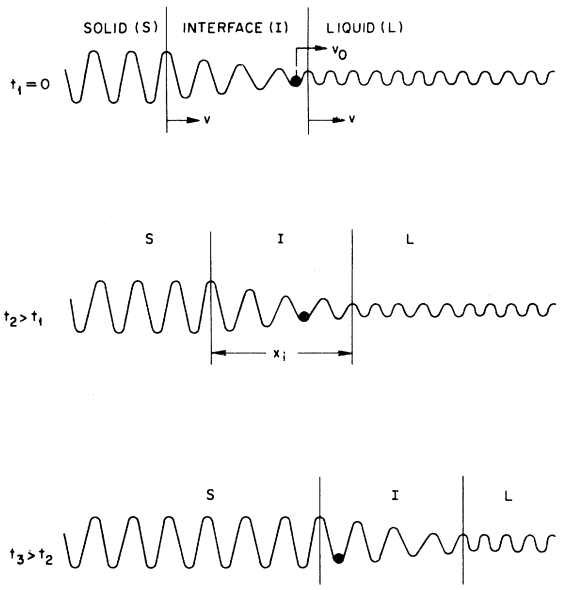

FIG. 1. Schematic illustration of a dopant atoms progression through the interface region.

In any case, a time-independent activation energy $U_d^r(v)$ can be obtained from an average of $U_d^r(v,t)$ over the time t_i the dopant atom spends in I. Of course, because of diffusion, t_i may be much longer than the time required for region I to pass a stationary point. The reader should realize that there is a great difference between the kinetics of interface processes for dopant and host atoms in a dilute solution. Host atoms are constantly undergoing transitions between the liquid and solid phases also, but whenever a host atom leaves the solid there is almost always another host atom at the interface to take its place, whereas this is not true for a dopant atom. A dopant atom has a high probability of being replaced by a host atom as a consequence of an interface exchange process. This probability is high (and therefore k_i is low) at low interface velocities where many interchanges occur before the interface passes.

Several simple forms for $U_d^r(v)$ have been investigated in the calculations to date. The two which have been used most often are

$$U_d^r(v)=U_d^{r0}+\Delta U_d^{ra}[1-\exp(-v/v_0)] , \tag{19a}$$

and

$$U_d^r(v)=U_d^{r0}+\Delta U_d^{ra}\{1-(v_0/v)\times[1-\exp(-v/v_0)]\} . \tag{19b}$$

For both forms, $U_d^r(v)$ goes to U_d^{ro} as $v\rightarrow 0$ and to $U_d^{r0}+\Delta U_d^{ra}$ as v becomes large, as required. Equation (19b) was obtained by time averaging (over t_i) the expression

$$U_d^r(v,t)=U_d^{r0}+\Delta U_d^{ra}[1-\exp(-vt/v_0t_i)] . \tag{20}$$

The quantity v_0t_i can be interpreted loosely as the distance x_0 the atom diffuses while in region I and v_0 can be related to an average diffusion coefficient D_i of the dopant in I by $D_i=v_0x_0$. Experimental values of D_i are probably completely unattainable, so in the calculations it will be assumed that $D_i\propto D_l$ and $x_0\propto x_0'$, with $v_0=D_l/x_0'$. An expression for $U_d^r(v,t)$ which yields Eq. (19a) is not as simple as Eq. (20), but its interpretation is basically the same.

The maximum value that $U_d^r(v)$ attains when v becomes very large will be denoted by U_d^{rm}; it is given by $U_d^{r0}+\Delta U_d^{ra}$. Considering the above discussion and Fig. 1, it seems reasonable that in a dilute solid solution U_d^{rm} should be approximately the activation energy U_d^s for impurity diffusion in the solid; therefore let us take

$$U_d^{rm}\equiv U_d^{r0}+\Delta U_d^{ra}=U_d^s . \tag{21}$$

Using Eq. 17, it is then found that

$$U_d^{ro}=U_d^s+kT_h\ln k_i^0 , \tag{22}$$

which can be used in Eqs. (19a) or (19b) to calculate numerical values of $U_d^r(v)$, if desired. When the solution is no longer dilute, U_d^{rm} will depend on the concentration in the solid and on the phase being formed and its interpretation may not be simple [see, e.g., the comments following Eq. (18)].

In the rest of this paper, the model developed above will be referred to as the VDAE (velocity-dependent activation energy) model.

C. Calculations of k_i for various dopants in silicon

Calculations of k_i (from Eqs. 17–19) at the present stage of development of the VDAE model are quite simple, but they involve input data which are not known at all for many dopants and are of

limited accuracy when they are available. For example, Trumbore[10] has estimated that there are probably errors of $\pm 10-20\%$ associated with even the most accurate measurements of the values of k_i^0 shown in Table I. The diffusion coefficients of group III and V dopants in liquid Si have been measured by Kodera[21] and by Shashkov and Gurivich[22] and their results are shown in Table I. It can be seen that there are substantial differences between the two sets of values and that Kodera has assigned rather large error limits to his values. The calculations of dopant diffusion during pulsed-laser annealing reported in Ref. 2 showed that the Kodera values gave consistently better results than those of Shashkov and Gurivich. In the calculations of this subsection (and of Ref. 3), values of D_l for the dopants considered by Kodera were allowed to vary only within the ranges given by him. The parameter v_0 of Eqs. (19a) and (19b) was expressed as D_l/x_0' and by trial and error values of x_0' and of D_l which gave reasonably good fits to the values of k_i shown in Table I were determined. The laser annealing conditions used in Ref. 15 were usually such that the average melt-front velocity was 4—4.5 m/sec (see Refs. 1 and 2), and the approximate fits to the experimental dopant profiles assumed values of v in this range for all dopants, except Sb where v was thought to be $\sim$3m/sec because of the longer pulse duration times used in the annealing.

Figures 2 and 3 show the results of calculations

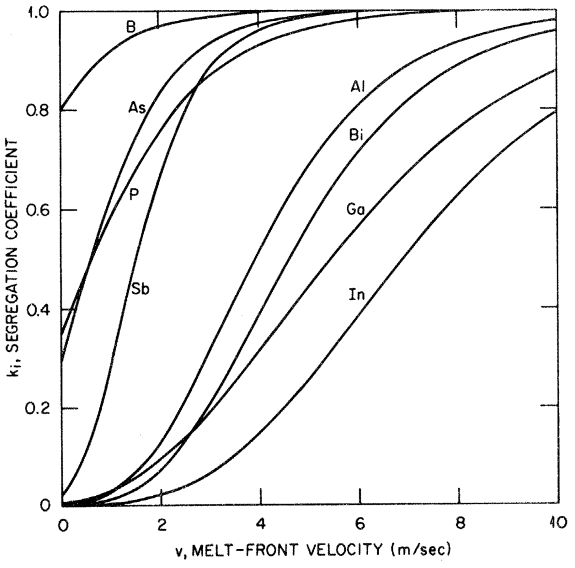

FIG. 2. Variation of k_i with v for group III and V dopants in Si using Eqs. (17), (18), and (19a).

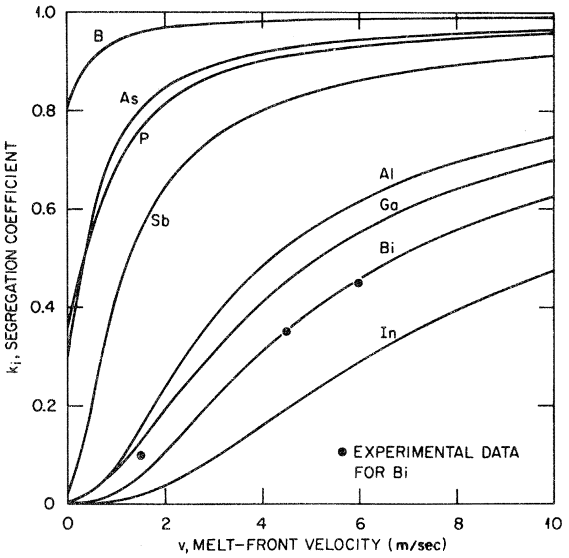

FIG. 3. Variation of k_i with v for group III and V dopants in Si using Eqs. (17), (18), and (19b).

of k_i for most of the group III and V dopants in Si as a function of v using Eqs. (19a) and (19b), respectively. At the time Ref. 3 was written, the calculated results were in somewhat better agreement with the values of k_i in Table I (at $v \simeq 4$ m/sec) for (19a) than for (19b). In the meantime, however, in another series of experiments White *et al.*[23] have used substrate heating[1,24] to control the melt-front velocity during the pulsed-laser annealing of Bi-implanted Si samples. From results such as those given by Wood and Giles in Ref. 24, they estimated the melt-front velocities to be $\sim$1.5, 4.5, and 6.0 m/sec for substrate temperatures of 650 K, 300 K, and 100 K, respectively. They then used these values of v to extract values of k_i from fits to the measured dopant profiles by the methods described in Refs. 15 and 2. The values of k_i found in this way were $\sim$0.1, 0.35, and 0.45 for $v \simeq 1.5$, 4.5, and 6.0 m/sec, respectively. Bismuth was one dopant for which D_l values were not given in either Refs. 21 or 22. If it is assumed that $D_l = 5.5 \times 10^{-4}$ cm^2/sec for Bi, the new data can be fit quite well with the VDAE model calculations when (19b) is used, as indicated in Fig. 3; in fact, the fit must be considered fortuitously good. Thus, at this point no clear-cut choice can be made between the two forms of Eq. (19).

The value of x_0' used in Eq. (19a) was 225 Å and in Eq. (19b) it was 850 Å. This may appear to be a rather large difference, but it must be empha-

sized that D_l cannot be the appropriate value of D_i, the average diffusion coefficient in the interface region. Values of D_i can be expected to lie between D_l and D_s (solid), although probably much closer to the values of D_l. Since the range between D_l and D_s covers about five orders of magnitude for the dopants considered here, good estimates of D_i cannot be made at this time. Thus, a difference of a factor of four in the values of x' when different forms of $U_d^r(v)$ are used cannot be of particular significance at this stage of our understanding of the processes in the interfacial region.

Table II shows some of the results of the calculations. The second column of Table II gives the values of ΔU_d^{ra}; this is a fixed quantity (for any particular dopant) and its significance will be discussed in more detail below. The third column shows the values of k_i obtained when a single value of v_0 for all dopants is used in Eq. (19a). These results demonstrate conclusively that the extraordinarily large departures of k_i from k_i^0 observed after pulsed-laser annealing can be accounted for by the VDAE model. The fourth column gives the results of calculations when Eq. (19a) was used and v_0 was made proportional to values of D_l within the ranges given by Kodera. These data achieve better agreement with the experimental data (Table I) than do those in column 3 and indicate that the values of D_i may indeed follow the trends in the values of D_l. In fact, it is interesting to note that if the dimensions of the interface region are of the order of an interatomic layer spacing in silicon ($\sim$2.5 Å), the values of D_i cannot be less than those of D_l by more than about two orders of magnitude if satisfactory values of $v_0 = D_i/x_0$ are to be obtained. If it is assumed that the interface region is of the order of 10 atomic layers, which does not seem unreasonable (especially if it is recognized that the likelihood of atomic layers going down in perfect order is remote), then the values of D_i need be less than those of D_l by only about an order of magnitude. The fifth column gives the values of D_l actually used in obtaining the curves of Fig. 3. The last column gives the values of k_i calculated using Eq. (19b). In carrying out the calculations with Eq. (19b), only two values of D_l were changed from those shown in the fifth column; D_l for Bi and In were assumed to be 5.5×10^{-4} cm^2/sec and 8.1×10^{-4} cm^2/sec, respectively. The latter value is still within the range given by Kodera and, as already mentioned, no values of D_l for Bi in Si have been given.

In assessing the agreement between the experimental and calculated values for k_i it must be kept in mind that both sets of results are subject to the same types of problems. The calculations which must be carried out to extract values of k_i from the experimental data involve values of D_l of limited accuracy, recrystallization velocities which are approximated by an average value (the results in paper I and Ref. 24 show that v actually changes somewhat during the recrystallization process), and solutions of the dopant diffusion equation with segregation treated in an approximate manner. The calculations with the VDAE model involve values of D_l of limited accuracy (which are only used as a guide to values of D_i), values of k_i^0 which have substantial uncertainties associated with them, and functional forms of $\Delta U_d^r(v)$ which can only approximate the correct form. With these considerations in mind, the agreement be-

TABLE II. Results of the calculations of k_i using Eqs. (19a) and (19b) in the expression for k_i [Eq. (18)]. Recrystallization velocities of 4 m/sec were assumed for all dopants except Sb for which v = 3 m/sec.

Dopant	ΔU_d^{ra} eV	k_i [Eq. (19a)] v_0=const	k_i [Eq. (19a)] $v_0=D_l/x_0'$	D_l [Eq. (19a)] 10^{-4} cm^2/sec	k_i [Eq. (19b)] $v_0=D_l/x_0'$
B	0.032	0.98	0.99	2.4	0.98
P	0.152	0.90	0.93	3.4	0.90
As	0.175	0.88	0.97	2.4	0.92
Sb	0.547	0.68[a]	0.88[a]	2.0	0.74[a]
Ga	0.700	0.61	0.31	6.3	0.41
In	1.134	0.45	0.15	6.4	0.16
Bi	1.053	0.48	0.39	4.4	0.31
Al	0.901	0.53	0.52	4.0	0.48

[a] v = 3 m/sec

tween experiment and theory must be considered satisfactory at this time. The results of the next two sections will further reinforce this conclusion.

Figure 4 shows values of k_i as a function of melt-front velocity for selected impurities over an extended range of the velocity. The curves for Cu, Au, and Ag clearly show the large differences obtained when Eqs. (19a) and (19b) are used. It is possible that the expressions in the parentheses of Eqs. (7c) and (7d) are no longer approximately unity at the higher velocities shown in Fig. 4. Nevertheless, it is of interest to see that with Eqs. (11) and (19a), k_i does very nearly reach 1 for Bi and In at velocities which may be attainable under some laser annealing conditions. In the calculations on Cu, Au, and Ag in Si, the values of k_i^0 shown by Trumbore were used and D_l was given a value of 8×10^{-4} cm^2/sec. With the same assumptions the calculated curves for Fe and Co fall just between those for Ag and Au, but they are not shown on Fig. 4 to avoid confusion. Because of some of the underlying assumptions of the model, the curves for the noble and transition metal impurities may be of only qualitative significance, especially at the higher melt-front velocities. However, in Sec. V it will be shown that the size of the segregation cells observed for Fe in Si are predicted fairly well by the values of k_i shown in Fig. 4.

Greater insight into the physical content of the VDAE model can be obtained by consideration of the energy of a dopant atom as it traverses the interfacial region between the liquid and the solid, and this will now be investigated.

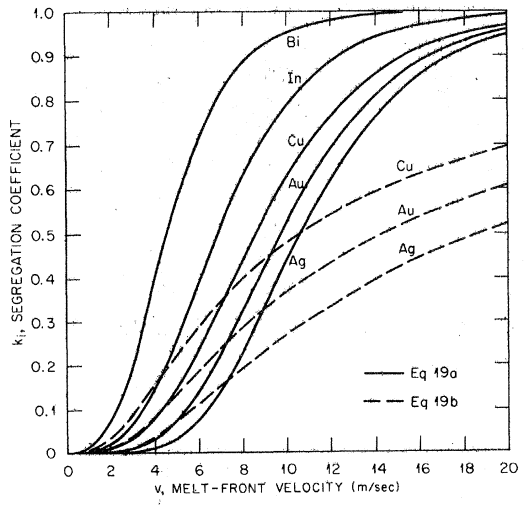

FIG. 4. Variation of k_i with v over an extended range of v for selected dopants using both Eqs. (19a) and (19b). See text for the details of this calculation.

D. Energy diagrams for dopant atoms

With certain of the results from above, and approximations frequently used in the literature, it is possible to construct semiquantitative energy diagrams for a dopant atom as it moves from the liquid, through the interface region, and into the solid. One of the difficulties in constructing such diagrams is to define energies which can be associated with individual atoms. To illustrate this difficulty and to set the scale of the energy diagrams, let us consider the following. The cohesive energy of a solid is the difference in energy of the collection of atoms forming the solid when the atoms are at infinite separation and when they are in the solid at $T=0$ K.[25,26] The sublimation energy (assuming complete separation into atomic species) is usually taken as the experimental measure of the cohesive energy. In a covalent material such as Si, the bonds between the nearest-neighbor atoms account for very nearly all of the cohesive energy[27] and therefore the cohesive energy can be used to obtain an estimate of the energy per covalent bond. In the silicon crystal structure, each covalent bond is shared by two atoms while each atom shares bonds with its four neighbors. The binding energy E_b^s of an atom in a solid is the energy required to remove the atom from the bulk of the solid (held at $T=0$ K) and to place it at infinity (with no kinetic energy). It is not difficult to see that for crystals with the Si structure, E_b^s can be approximated by twice the sublimation energy per atom $E_{\rm sub}$, e.g., for Si,

$$E_b^s(\mathrm{Si})\simeq 2E_{\rm sub}(\mathrm{Si})\ . \tag{23}$$

In a similar manner the binding energy of a Si atom in the liquid $E_b^l(\mathrm{Si})$ is given by

$$E_b^l(\mathrm{Si})=2[E_{\rm sub}(\mathrm{Si})-E_F(\mathrm{Si})]\ , \tag{24}$$

where E_F is the latent heat of fusion per Si atom. On the schematic energy diagrams displayed in Fig. 5, the zero of energy is taken as the energy of a perfect Si crystal plus a single Si atom at infinity. If the Si atom is added to the solid the total binding energy of the system is increased by $E_b^s(\mathrm{Si})$ and if the atom is added to the liquid, the binding energy is increased by $E_b^l(\mathrm{Si})$; vibrational energies

are not included in these quantities.

Next let us assume that a Si atom has been replaced by a dopant atom, such as As, which has strong covalent bonding with the Si host. Following the procedure used by Weiser,[28] which is based on an approximation suggested by Allen,[29] the binding energies of group III and V dopants in solid Si can be estimated from the equation

$$E_b^s(d)=\left[\frac{1}{4}\left[\frac{1}{E_{\rm sub}(d)}+\frac{1}{E_{\rm sub}({\rm Si})}\right]\right]^{-1} . \tag{25}$$

in which $E_{\rm sub}(d)$ is the sublimation energy of the pure dopant crystal. For simplicity, it will be required that

$$E_b^s({\rm Si})-E_b^s(d)=E_b^l({\rm Si})-E_b^l(d) , \tag{26}$$

from which it follows that

$$E_b^l(d)=E_b^s(d)-2E_F({\rm Si}) . \tag{27}$$

A better estimate for $E_b^l(d)$ could undoubtedly be made by some modification of the ideas leading to Eq. (25), but this seems an unwarranted complication at this time.

Having established a scale for the binding energies, the activation energies for diffusion of the dopant atoms can be displayed on the same diagram. Activation energies for diffusion of many impurities in solid Si [U_d^s of Eq. (21)] have been reported in the literature[30] but none in liquid Si have appeared. Rough estimates of U_d^l, the activation energy for impurity diffusion in the liquid, can be made as follows. The diffusion coefficients in the solid are given in the form

$$D_s=D_s^0\exp(-U_d^s/kT) , \tag{28}$$

and presumably by a corresponding form in the liquid. The preexponential factors will be assumed to be the same in the solid and liquid, i.e., $D_l^0=D_s^0$ (an obvious oversimplification); then

$$\ln(D_s/D_l)=-(U_d^s-U_d^l)/kT_n . \tag{29}$$

Even if D_s^0 is greater than D_l^0 by a factor of two or three it will not greatly change the estimates of U_d^l arrived at. In fact, as already discussed, it is not D_l but the *effective* diffusion coefficient in the interface region D_i which is needed in the VDAE model. Nevertheless, estimates of U_d^l are of interest for illustrative purposes.

Before constructing the energy diagrams it is useful to have one other piece of information. The ratio of rate constants for the solidification of an undoped host is usually written[31] in terms of the molar latent heat of fusion as

$$K_h^f/K_h^r=(A_h^f/A_h^r)\exp[(U_h^f-U_h^r)/RT]$$
$$=(A_h^f/A_h^r)\exp(L_h/RT) . \tag{30}$$

The ratio A_h^f/A_h^r is determined by noting that at the melting temperature T_h the liquid-solid interface in the pure host material is not moving ($v=0$) and hence $K_h^f/K_h^r=1$ [Eq. (9)]; therefore,

$$A_h^f/A_h^r=\exp(-L_h/RT_h) . \tag{31}$$

Since the A's and U's are assumed to be independent of temperature, Eq. (30) can be written as

$$K_h^f/K_h^r=\exp[(L_h/R)(T^{-1}-T_h^{-1})] . \tag{32}$$

This expression can be converted to one applying to a single host atom transferred between the liquid and solid by setting

$$K_h^f/K_h^r=\exp\{[2E_F({\rm Si})/k](T^{-1}-T_h^{-1})\} . \tag{33}$$

E_F(Si), the latent heat per atom, appears with a factor of 2 in Eq. (33) because the total energy change of the system has been associated with the transferred atom. Consistent with previous assumptions, we now have

$$A_d^f/A_d^r=A_d^{fo}/A_d^{ro}=A_h^{fo}/A_h^{ro}$$
$$=\exp[-2E_F(h)/kT_h] , \tag{34}$$

and, as a special case of Eq. (11),

$$k_i^0=K_d^{fo}/K_d^{ro}$$
$$=\exp[-2E_F(h)/kT_h]$$
$$\times\exp[(U_d^{ro}-U_d^{fo})/kT] . \tag{35}$$

This form, which follows simply from the approximations that have been made, is of no special significance in itself, but it can be used to obtain Eq. (37) below. To see this, let us consider again the case that $k_i\to 1$ as $v\to\infty$, and $T\simeq T_h$. Using Eqs. (17), (21), and (35), we obtain

$$\Delta U_d^{ra} = U_d^s - U_d^{r0}$$
$$= -kT_h[-2E_f(h) + U_d^{r0} - U_d^{f0}]/kT_h \tag{36}$$

or

$$U_d^{f0} = U_d^s - 2E_F(h) \ . \tag{37}$$

It may seem peculiar that the effective activation energy for transitions from the liquid to the solid should involve U_d^s explicitly, but it should be kept in mind that all of the activation energies have been deliberately related to U_d^s, which is considered to be known with fair accuracy.

Equations (23)—(25), (27), (29), and either (19a) or (19b) provide the relationships needed to construct the energy diagrams. The data used in the calculations are given in Table III for the common group III and V dopants in silicon. Values of D_s^0 and U_d^s were taken from the compilation of Sharma,[30] where references to the original literature can be found. Measurements of diffusion coefficients over a range large enough to include the melting point are rarely ever made because of the obvious experimental difficulties in collecting data near $T = T_h$. Nevertheless, Eq. (28) was used to estimate $D_s(T_h)$ from the information in Ref. 30. Two sets of values for D_s^0, U_d^s, and U_d^l have been given for some dopants to illustrate the variations in these quantities from various sources given in Ref. 30. Values of the sublimation energies were taken from the tabulation of Stull and Sinke[32] and from Table I of Chapter 3 in Ref. 26. For Si, $E_b^s(\text{Si}) \simeq 9.25$ eV and $E_b^l(\text{Si}) \simeq 8$ eV.

Table III shows that for the group III and V dopants in Si, values of U_d^s, U_d^l, and $E_b^s(d)$ fall within a fairly limited range and on schematic diagrams such as those in Fig. 5 there is little point in indicating the differences. It is in the values of the *effective* activation energies $U_d^r(v)$ of Eqs. (19a) and (19b) that major differences show up and demonstrate how the model functions. This is illustrated in the two diagrams of Fig. 5 by the dashed curves in region I which represent $U_d^r(v)$ calculated from Eq. (19a) for various velocities. The right-hand portion of the uppermost curve in both diagrams has been made solid to indicate the value of U_d^{fo}, which is given by Eq. (37) and is not velocity dependent. The maximum height obtained by the dashed curves cannot exceed that of the solid curve and equality may be achieved only as v becomes large. In Fig. 5(a) the dashed curves show the rapid increase of $U_d^r(v)$ as a function of v for dopants such as As, and B, and P. For these dopants $U_d^r(v)$ and K_i have very nearly reached their maximim values [see Eq. (21) and Fig. 2] for $v \simeq 4$ m/sec. Figure 5(b) illustrates the much more gradual increase in $U_d^r(v)$ with v for dopants such as Bi and In. For these dopants $U_d^r(v)$ and k_i do not reach their maximum values until $v \simeq 12$ m/sec

TABLE III. Data for the construction of dopant energy diagrams. The symbols are explained in the text; see also Fig. 5.

Dopant	D_d^{s0} (cm^2/sec)	U_d^s (eV)	U_d^l (eV)	$E_{\text{sub}}(d)$ (eV/atom)	$E_b^s(d)$ (eV)
B	16	3.69	1.61	5.81	10.32
	25	3.51	1.67		
P	10.5	3.69	1.44	3.95	7.90
As	0.32	3.56	1.00	3.0	7.28
	68.6	4.23	1.78		
Sb	5.6	3.95	1.52	2.7	6.82
	12.9	3.98	1.65		
Ga	3.6	3.51	1.29	2.78	6.96
In	16.5	3.9	1.33	2.6	6.66
Bi	10.30	4.64	2.13	2.15	5.88
Al	8	3.47	1.35	3.34	7.76

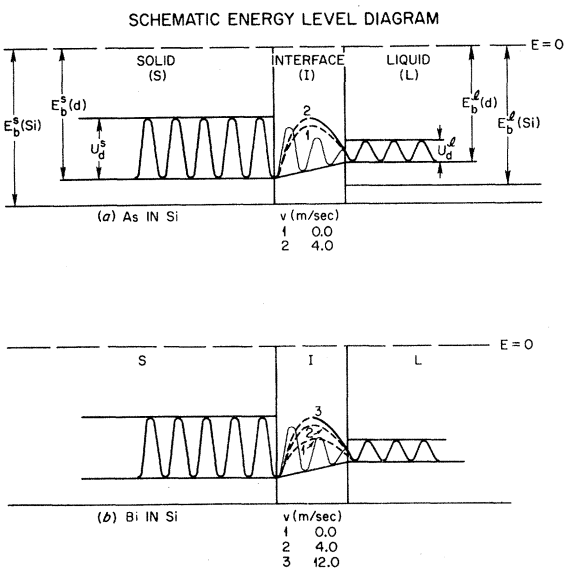

FIG. 5. Schematic diagram of the energy of a dopant ion in the liquid, interface, and solid regions. This diagram is discussed in detail in the text.

[using Eq. (19a)].

It can be seen from the energy diagrams in Fig. 5 that the VDAE model works in the following manner. A dopant atom in the liquid (assumed to be at temperature T_h) requires an effective activation energy of $U_d^{fo}=U_d^s-2E_F(h)$ to make a transition into the solid; U_d^{fo} does not depend on the liquid-solid interface velocity and therefore applies also when $v=0$. Once the dopant atom is "in the solid" it requires an effective activation energy of $U_d^r(v)=U_d^{r0}-kT_h\ln k_i^0 f(v)$ to make a transition back into the liquid. When $v=0$, $U_d^r(0)=U_d^{r0}$, which is the minimum value that $U_d^r(v)$ can have, and hence k_i takes on its minimum value, i.e., k_i^0. As the velocity increases, $U_d^r(v)$ increases thus decreasing the rate at which dopant atoms make a transition from the solid into the liquid, and hence k_i increases. When $v\to\infty$ and $U_d^r(v)\to U_d^s$, the potential barrier against a transition back into the liquid exceeds U_d^{f0} by $2E_F(h)$. It might seem that k_i should go to unity when $U_d^r(v)=U_d^{f0}$, but Eq. (11) shows that it is the rate constants and not the activation energies which determine k_i. Also, the reader is cautioned against associating the activation energies with chemical potentials; this will be discussed in more detail in Sec. VI.

The energy diagrams described in this subsection are of use in obtaining a qualitative (and even semiquantitative) estimate of the energy of a dopant atom as it goes back and forth between the idealized solid and liquid regions; however, the diagrams are incomplete as far as the solidification process itself is concerned. The heat transfer calculations of paper I show that there are very large temperature gradients across the interface region and in the solid itself; the temperature gradients in the liquid are much smaller. Thus, a dopant atom after traversing the interface region will not find itself at the botton of one of the potential wells shown in the solid region of Fig. 5, but will be in a highly excited vibrational state. In this connection, it should be noted that Eq. (35) has been used to relate U_d^{f0} to U_d^s and is not an equation for calculating k_i^0 because U_d^{r0} remains undetermined. Similarly, Eq. (22) gives a relationship between U_d^{r0} and k_i^0 which must hold for the internal consistency of the model, but it does not provide a method for calculating either quantity.

IV. SOLUBILITY LIMITS

By requiring that $k_i\to 1$ as v becomes large, it is virtually ensured that complete incorporation of the dopant into the solid will always occur at sufficiently high crystallization velocities [subject, of course, to the limitations imposed by Eq. (9) and the rate constants]. However, the definition of k_i [Eq. (7a)] is noncommittal about the phases which form in the liquid (or in the interface region) or which subsequently appear in the solid behind the interface. If one examines the theory of one-dimensional solidification due to a moving melt front,[11] it is also seen that there is nothing in the theory which specifies the phases appearing in the liquid or the solid. Moreover, the theory does not require that a crystal lattice be formed or that the processes occur near thermodynamic equilibrium, i.e., k_i need not be k_i^0. All information of a thermodynamic nature has to be incorporated into the theory in a somewhat *ad hoc* manner. When crystallization is slow enough that thermodynamic equilibrium holds locally, this can be done with some assurance. When local equilibrium is known not to hold, the entire problem becomes much more complex, as we have already seen above. The identification of $U_h^f-U_h^r$ with the latent heat of fusion in Eq. (30) is an example of the process by which thermodynamic information is related to quantities appearing in the kinetic theory of solidification. Of course, the relationships between kinetic theory, thermodynamics, and crystal growth have been discussed often in the literature,

but almost invariably the authors appear to assume implicitly that the processes are occurring near thermodynamic equilibrium (e.g., at very low solidification velocities).

In a purely thermodynamic approach, the equilibrium segregation coefficient k_i^0 for a binary alloy is referred to the phase diagram and identified with the ratio of the concentration of solute atoms at the solidus to that at the liquidus for a given temperature. For convenience, ideal, dilute solutions are usually assumed in both the liquid and solid phases, although corrections for real solutions and higher concentrations can be made. In this section, a simple approach, following along lines often discussed in the literature,[31] is taken to investigate the increase of solubility with melt-front velocity to be expected from the VDAE model of the pulsed-laser annealing process.

For an ideal, dilute, binary solid solution which is crystallizing from an ideal, saturated, liquid solution, the molar concentration of the host in the liquid is

$$C_h^l = \exp[-L_h(T_h - T)/RT_h^2] \,. \tag{38}$$

This expression can be obtained, for example, from Eq. (4.6) of Ref. 31 under the assumption that T is not greatly different from T_h, the melting temperature of the host material. Also, from Eq. (4.33) of Ref. 31

$$v/K_h^r = L_h(T_h - T)/RT_h^2 \tag{39}$$

(recall that L_h is the molar latent heat of h and K_h^r is the reverse rate constant for h). Then, since

$$C_d^s = k_i C_d^l = k_i(1 - C_h^l) \,. \tag{40}$$

we have that

$$C_d^s = k_i[1 - \exp(-v/K_h^r)] \,. \tag{41}$$

When v is much smaller than K_h^r, as will usually be the case, the exponential can be expanded and the very simple expression

$$C_d^s = k_i(v/K_h^r) \tag{42}$$

obtained. Equation (41) gives a simple estimate of the maximum concentration of dopant which will appear in the solid solution (i.e., substitutionally for the III and V dopants in Si) at a given crystallization velocity. Of course, the equation does not predict an absolute solubility limit because the assumption on which it is predicated cannot hold at arbitrarily high concentrations and recrystallization velocities.

Table IV shows some of the quantities related to the calculations of C_d^s/C_d^{s0} which have been made following the simple theory outlined above. The second column gives values of the maximum equilibrium concentration in atoms/cm^3 extracted by the authors of Ref. 15 from Fig. 2 of Trumbore's compilation. In the third column, these values have been converted to atomic percent by assuming that there are 4.9×10^{22} Si atoms/cm^3, which corresponds to a silicon density of 2.3 g/cm^3. Columns four and five give experimental data taken directly from Ref. 15. Values of C_d^s calculated from Eq. (42) using the values of k_i shown in Table II are listed in columns six and seven. The interface velocity was taken equal to 4 m/sec for all dopants except Sb for which it was 3 m/sec to correspond to the conditions of Ref. 15. The rate constant K_h^r was assumed to be 100 m/sec. The fifth and six columns show values of the ratio C_d^s/C_d^{s0} which follow from the data in

TABLE IV. Experimental data and results of calculations of the solubility limits using Eq. (42). Calculations were made with values of k_i from both Eqs. (19a) and (19b). The recrystallization velocity was taken to be 4 m/sec except for Sb where 3 m/sec was used.

Dopant	N_d^{s0} (Ref. 10)	C_d^{s0} (Ref. 10)	N_d^s (Ref. 15)	C_d^s/C_d^{s0} (Ref. 15)	C_d^s [Eq. (19a)]	C_d^s [Eq. (19b)]	C_d^s/C_d^{s0} [Eq. (19a)]	C_d^s/C_d^{s0} [Eq. (19b)]
B	6.0×10^{20}	0.0122			0.0396	0.0392	3.2	3.2
P	1.4×10^{21}	0.029			0.0372	0.0360	1.3	1.2
As	1.5×10^{21}	0.031	6.0×10^{21}	4	0.039	0.037	1.3	1.2
Sb	7.0×10^{19}	0.0014	1.3×10^{21}	18	0.0264	0.0220	19.0	16.0
Ga	4.5×10^{19}	0.00092	4.5×10^{20}	10	0.0124	0.0164	13.5	18.0
In	8.0×10^{17}	0.000016	1.5×10^{20}	188	0.0060	0.0064	375.0	400.0
Bi	8.0×10^{17}	0.000016	4.0×10^{20}	500	0.0156	0.0124	975.0	775.0
Al	2.0×10^{19}	0.00041			0.0208	0.0192	51.0	47.0

columns 3, 6, and 7.

The agreement between experiment and theory is certainly acceptable when one considers the various uncertainties to which both the experiments and calculations are subject. However, there are a few comments which need to be made about the results. White *et al.*[15] show $N_d^0=8\times10^{17}$ cm^{-3} for the case of In in Si and seem to imply that this value comes from Trumbore's compilation; in fact, all Trumbore states is that the value of N_d^0 for In is probably $<4\times10^{17}$. Also, Fig. 12 of Ref. 15 appears to indicate that the measured value of the maximum concentration in In should be approximately 2.0×10^{20} rather than 1.5×10^{20}, as shown here and in Table III of the same reference. In that case, the experimental value of C_d^s/C_d^{s0} could be as high as ~500 rather than the 188 shown in Ref. 15; this would significantly improve the agreement between the measured and computed values. The calculated value of C_d^s/C_d^{s0} for Ga is significantly higher than the measured value. Approximately 50% of the Ga was lost during the laser annealing and this makes an accurate determination of k_i difficult. Also, the calculations of k_i seem to be consistently too high and this may mean that Kodera's value of D_l for Ga is substantially in error or is not a good indication of the value of D_i needed in the calculation of k_i. Ironically, the greatest percentage disagreement between theory and experiment is for arsenic, which should be well-behaved because its atomic radius is very close to that of silicon. This disagreement probably occurs because the assumptions leading to Eq. (42) are overly simplified. It should be noted that Eqs. (41) and (42) make $C_d^s\to0$ as $v\to0$ and this cannot be correct. For dopants with small values of k_i^0 this is of little importance, but for dopants such as As which have large values of k_i^0 an expression which behaves properly at small v would be useful. Such an expression might also affect the choice of K_h^r for which the value of 100 m/sec may seem rather high to some readers. Finally, it should be noted that the value of N_d^s observed for As means that $C_d^s\simeq0.12$, and therefore the concentration of dopant atoms can no longer be considered dilute.

V. CELLULAR STRUCTURE

Formation of cellular structure due to the breakdown in stability of a planar melt front during the solidification of materials is a well-known phenomenon.[33] In the laser-annealing experiments, the cellular structure consists of regions of host material containing the solute or dopant atoms at relatively low concentrations surrounded by the cell walls in which the concentration of dopant is much higher. Clearly, the questions of the dependence of the solubility on interface velocity and the solubility limits which are ultimately attainable are closely related to the question of how the stability of the planar interface is influenced by the various physical parameters entering into the problem.

A. Review of the Mullins and Sekerka theory of cellular structure

Mullins and Sekerka[4] have given an elegant formulation and solution of the interface stability problem by considering the effects of a sinusoidal perturbation imposed on the planar interface. The interested reader should study Ref. 4 for the details of the Mullins-Sekerka (MS) treatment, but here it seems appropriate to discuss briefly the three major assumptions underlying that treatment. The first assumption is that steady-state solidification has been attained and that mass (dopant) and heat transport can be described by the appropriate conventional diffusion equations[11] (no convection). The use of diffusion equations to describe redistribution of dopants in the molten material is in accord with the melting model of pulsed-laser annealing, but it frequently happens that steady-state conditions are not attained for some dopants in the shallow surface region melted by the laser radiation (see Ref. 2). The second assumption imposed by Mullins and Sekerka is that the sinusoidal perturbation is sufficiently weak that its effects on the dopant concentration and temperature distributions a few wavelengths from the moving liquid-solid interface are completely negligible.

The third assumption of the MS treatment consists of two boundary conditions imposed at the liquid-solid interface. The first condition is of particular interest here because it relates the temperature at the interface to the liquidus curve on the phase diagram. Let T_ϕ be the temperature of the sinusoidally varying interface when the solute is present and T_N the temperature in the absence of the solute. Then the MS theory requires that

$$T_\phi=mC_{d,\phi}^l+T_N\ , \tag{43}$$

in which m is the slope (including sign) of the liquidus line on the phase diagram and $C_{d,\phi}^l$ is the

dopant concentration in the liquid at the interface. T_N is assumed to be related to the melting temperature of the host T_h for a planar interface condition by the capillary (surface tension) formula

$$T_N = T_h + T_h \Gamma K' . \tag{44}$$

In this relationship, K' is the average curvature at a point of the interface and Γ is a capillary constant. For the purposes of this paper, the important point about Eq. (43) is that m is the slope of the liquidus line and local equilibrium is assumed to hold *in the liquid;* nothing is assumed about the thermodynamic conditions *in the solid.*

The second condition to be satisfied at the interface requires that the interface velocity used in the dopant diffusion calculations must be consistent with the velocity obtained from the heat diffusion equations. This condition is expressed by

$$v(z) = \frac{1}{L_h}\left[K_s\left[\frac{\partial T_s}{\partial x}\right]_\phi - K_l\left[\frac{\partial T_l}{\partial x}\right]_\phi\right] = \frac{D_d^l}{C_{d,\phi}^l(k_i-1)}\left[\frac{\partial C_d^l}{\partial x}\right]_\phi , \tag{45}$$

in which K_s and K_l are the thermal conductivities of the pure host in the solid and liquid states, respectively, T_s and T_l are the corresponding temperatures and all other symbols have been previously defined; the subscript ϕ means that the quantities involved are to be calculated at the sinusoidally varying interface. The partial derivatives in Eq. (45) indicate that the interface is assumed to be moving in the x direction. The dependence of v on z comes about because the interface is no longer planar once the sinusoidal perturbation has been superimposed, and hence the velocity varies from point to point on the interface. Of course, v will depend on y also, but the extension to include this dependence is trivial, as Mullins and Sekerka point out. The relationship between the velocity of a melt front and the thermal gradients is well known; it is just an expression for the heat-flow equation. The relationship between the velocity and the derivative of the dopant concentration comes from an expression apparently first derived by Tiller *et al.*[34] but now found frequently in the literature. This expression if just the *steady-state* solution of the dopant diffusion equation for the case in which the initial dopant concentration C_d^{l0} is uniform and the melt-front moves with constant velocity; the solution is

$$C_d^l(x) = C_d^{l0}\left[1 + \frac{(1-k_i)}{k_i}\exp(-vx/D_l)\right] , \tag{46}$$

in which x is measured relative to the moving liquid-solid interface. The boundary condition at the interface is $C_d^l(0) = C_d^{l0}/k_i$ and at $x = \infty$, $C_d^l(\infty) = C_d^{l0}$. Differentiation of Eq. (46) and use of the interface boundary conditions gives the relationship between velocity and concentration at the interface expressed in Eq. (45). It appears that Mullins and Sekerka meant for k_i in Eq. (46) to be the equilibrium interface segregation coefficient, i.e., k_i^0 in the notation of this paper, but there is nothing in the derivation of Eq. (46) that restricts k_i to be k_i^0. This is an important point and together with the fact that Eq. (43) involves only the slope of the liquidus implies that the MS treatment is not restricted to conditions of thermodynamic equilibrium. More serious objections to applying the theory to the laser annealing of ion-implanted samples might be that (1) the initial concentration of dopant will generally not be uniform, and (2) for low values of k_i steady-state conditions will not be attained before the solidification front reaches the surface of the sample.

In any case, the central result of the MS theory is an expression for the time derivative of the infinitesimal sinusoidal perturbation of the interface [Eq. (20) of Ref. 4]. Analysis of this expression shows under what conditions instability of the planar interface is expected to occur. The analysis also provides an estimate of the cell size, but Mullins and Sekerka point out that in general the theory cannot be expected to give reliable predictions concerning the cell size unless the instability is known to be weak. Cahn *et al.*[35] have applied the MS theory to an analysis of cellular formation under conditions which they apparently felt applied to the ultrarapid crystallization characteristic of pulsed-laser annealing. However, they did not have available to them at the time certain experimental and calculated data which would have undoubtedly influenced their application of the MS theory. In particular, the experimental data which are now available show that the stability against cellular formation is much greater than predicted in Ref. 35 and that the predicted cell sizes are considerably different from those actually observed. The thermal gradients at the interface assumed by Cahn *et al.* are much smaller than those calculated by Wood and Giles,[1] but the most serious short-

coming of their calculations is the assumption that local equilibrium has to apply in the MS treatment and that as a consequence equilibrium or near-equilibrium values of the segregation coefficient should be used. As mentioned above, this is an unnecessary assumption, and Narayan[36] found that when he used in the MS theory values of k_i given by White *et al.*[15] and/or the expression for k_i given by the present author in ref. 3, he obtained fairly good agreement with his experimental data. The results of calculations which clearly show this to be the case will now be presented and discussed.

B. Calculations pertaining to cellular structure

Figures 6 and 7 show the results of stability calculations with Eq. (20) of Ref. 4 for Sb and In in Si, respectively. The two dark solid curves on each figure give the demarcation lines between stable and unstable regions of the plots of concentration vs melt-front velocity. The lower curve was calculated with $k_i = k_i^0$ and the upper curve with $k_i = k_i(v)$ given by Eqs. (17), (18), and (19a) using exactly the same data used to generate the curves

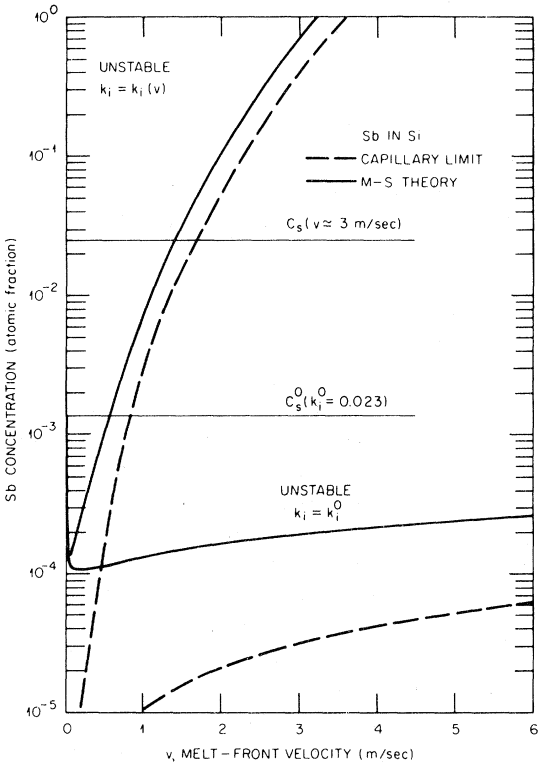

FIG. 6. Results of an interface stability calculation for Sb in Si following the Mullins and Sekerka theory and using values of k_i calculated with Eq. (19a).

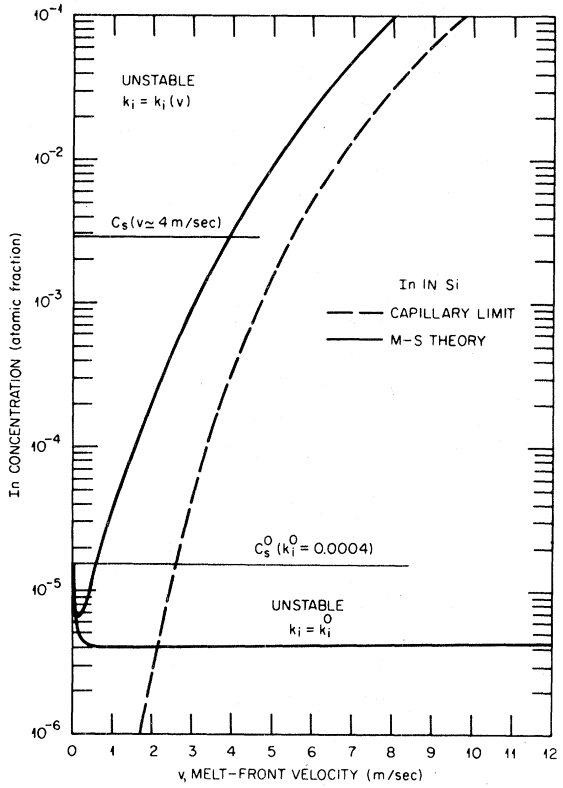

FIG. 7. Stability results for In in Si following the same procedure that led to Fig. 6.

of Fig. 2. Values of m (slope of the liquidus curve) were estimated from the phase diagrams of Sb and In in Si and the capillary parameter was taken from Ref. 35. The dashed curves in the figures give the "capillary limit" for which

$$C_d^s = \frac{k_i^2 T_h \Gamma v}{m(k_i - 1) D_l} \tag{47}$$

[see Eq. (27) of Ref. 4]. This is an absolute stability criterion which holds when the capillary effect completely dominates the effects of constitutional supercooling due to the presence of the solute. The thermal gradient or constitutional supercooling limit given by (see Ref. 35)

$$C_d^s = \frac{D_l k_i G_L}{m(k_i - 1) v} \tag{48}$$

represents the opposite extreme; these curves do not appear in Fig. 6 because they lie so close to the ordinate on the scale chosen. The light horizontal line, labeled C_s^0 ($k_i^0 = 0.023$), in Fig. 6 gives the equilibrium solubility limit ($v \simeq 0$) estimated from the compilation of Trumbore (see Table IV). The

other horizontal line, labeled C_s ($v \simeq 3$m/sec), indicates the approximate nonequilibrium concentration given in Ref. 15. The corresponding lines on Fig. 7 were obtained in the same manner, but with $v = 4$ m/sec for In in Si. It should be realized that because $k_i \rightarrow k_i^0$ as $v \rightarrow 0$, the stability curves for $k_i = k_i(v)$ and $k_i = k_i^0$ must go to the same values as $v \rightarrow 0$.

From Fig. 6 it can be seen that when $k_i = k_i(v)$, no cellular structure is expected to appear at $v = 3$ m/sec for the concentrations of Sb used thus far in the experiments. On the other hand, if at $v = 3$ m/sec, k_i had the equilibrium value of k_i^0, the planar melt front would be unstable against cellular formation at a concentration more than an order-of-magnitude lower than for $k_i = k_i(v)$. No cellular structure has been reported yet for laser-annealed samples of Sb-implanted Si and the agreement between experimental and calculated [Eq. (42)] values of $C_s/C_s^0 (\equiv C_d^s/C_d^{s0})$ is good, as indicated in Table IV.

In the case of In in Si, shown in Fig. 7, the ratio of C_d^s/C_d^{s0} observed experimentally was reported to be 188, whereas the calculated values shown in Table IV are higher. It can be seen from Fig. 7 that the line for $C_s \simeq 0.003$ atomic fraction crosses the $k_i = k_i(v)$ stability curve at $\simeq 4$ m/sec. Thus, small errors in the melt-front velocity and/or concentration of dopant could account for the factor-of-2 discrepancy which does exist between the experimental and calculated C_d^s/C_d^{s0} ratios. Also it should be recognized that when cellular formation does occur the amount of dopant left within the cells is not necessarily the maximum that can be placed substitutionally in the lattice at the particular crystallization velocity. The MS theory does not give quantitative information about the concentration in either the cells or the cell walls. It would seem that the correct way to establish the maximum concentrations is to approach the instability curves in Figs. 6–8 from below, i.e., by keeping the velocity fixed and gradually increasing the concentration until the instability just sets in. Of course, this would also be the best method for establishing the critical cell sizes discussed below. For this reason, the concentrations given by White *et al.*[15] are not necessarily the maximum ones that can be attained at the velocities they used.

Figure 8, which is quite similar to Fig. 6 and 7, shows the stability diagrams for Bi in Si using both Eqs. (19a) and (19b) in the calculations of k_i. Both stability curves with $k_i = k_i(v)$ predict that at $v = 4$–4.5 m/sec, no cellular structure should be

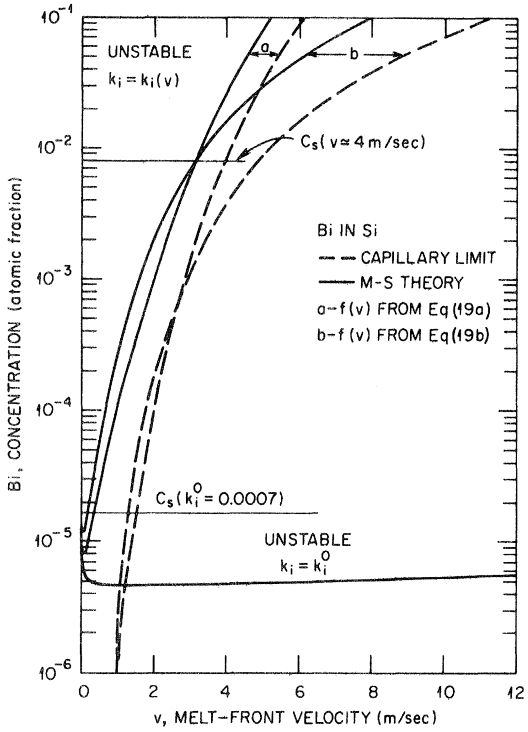

FIG. 8. Stability calculations for Bi in Si using the Mullins and Sekerka formulation; the results obtained using both Eqs. (19a) and (19b) are shown.

observed for Bi in Si at the maximum concentration employed in the experiments of Ref. 15. Experimental conditions for which cellular structure appears in the laser-annealed Bi-Si system have not been reported as far as this writer knows. However, the results shown on Fig. 8 suggest that, for the same ion-implantation conditions used in Ref. 15, use of substrate heating to slow the melt-front velocity to ~ 2 m/sec should lead to cellular formation. Of course, annealing of samples with sufficiently high implantation doses without substrate heating should also produce cellular formation.

The calculations which lead to the curves displayed in Figs. 6–8 also provide information about the dependence of the cell size on various parameters. In Fig. 9, the cell size at the onset of the interface instability is shown as a function of melt-front velocity. It can be seen that the cell size initially decreases rapidly with velocity and then goes into a region of much slower decrease. The concentrations corresponding to these cell sizes can be taken from curves like those of Figs. 6–8. It may be somewhat difficult experimentally to determine critical cell sizes to compare with the

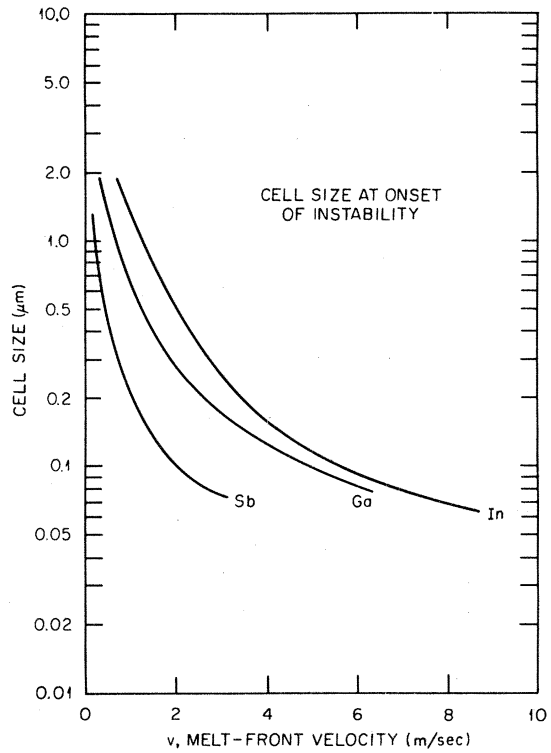

FIG. 9. Cell size at the onset of the interface instability as a function of melt-front velocity for Sb, Ga, and In in Si using k_i determined from Eq. (19a). The critical cell size *decreases* and the critical concentration *increases* (see Figs. 6 and 7) with v.

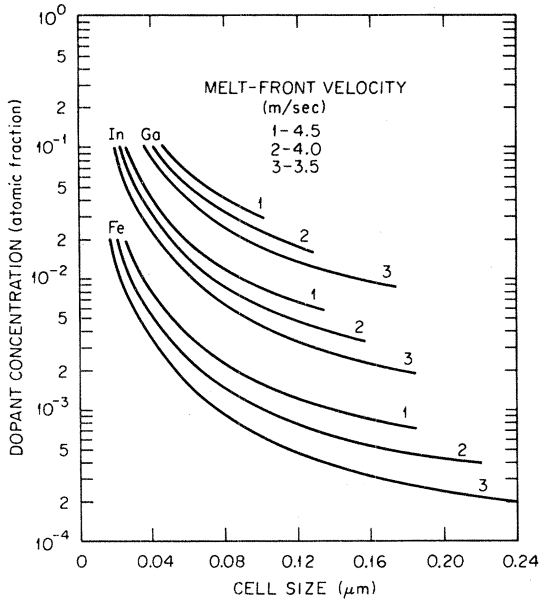

FIG. 10. Interrelationship of dopant concentration, melt-front velocity, and cell size. The cell size furthest to the right for a given velocity occurs at the onset of the instability. If the concentration is held fixed the cell size *increases* as the velocity is increased until, for a given veolcity, the interface becomes stable.

calculated values because of the difficulty in preparing samples with the correct concentrations and in establishing laser-annealing conditions which give exactly the right melt-front velocities to map out the boundary between the stable and unstable regions. Moreover, Fig. 9 shows that for v in the range of 4 m/sec, the critical cell size is less sensitive to the velocity than it is at lower values of v.

The curves displayed in Fig. 10 give information of a somewhat different type. To construct these curves, a melt-front velocity is chosen and the dopant concentration at which a particular cell size appears is determined. For example, in Fig. 7, let us suppose that 4 m/sec has been chosen for v and then determine the cell size for each concentration above the critical concentration for instability. This leads to curve 2 for the In group of curves on Fig. 10. The point furthest to the right on each curve on fig. 10 corresponds to the cell size and dopant concentrations at the onset of the interfacial instability. It should be noted that if one holds the concentration fixed and increases the melt-front velocity, the cell size *increases* up to a certain maximum value corresponding to that at which the stability curve (Figs. 6—8) is crossed. It is apparent from Fig. 10 that for a given concentration, the increase in cell size is very rapid as the velocity approaches that of the stability curve. As already mentioned above, this means that reliable values of the cell size at the onset of the instability will be difficult to determine experimentally.

The main point in presenting Figs. 6—8 is to demonstrate how the VDAE model leads to results which are in satisfactory agreement with the experimental data and to show the reader that calculations using k_i^0 in the MS formalism give results which differ from the observed data by orders of magnitude. As stated earlier, Mullins and Sekerka cautioned against the reliability of predictions about cell sizes unless the instability is known to be weak. However, from the sparse data that is now available, it appears that the predictions of cell size are perhaps more accurate than might be expected. Narayan[36] has reported cell diameters of 700 Å, 520 Å, and 350 Å respectively for Ga, In, and Fe in Si after laser annealing with pulses which should have produced melt-front velocities of approximately 4 m/sec. In fact, the Ga and In sam-

ples were the same as those used by White *et al.* (see Figs. 11 and 12 of Ref. 15) in their experiments. The concentration of In in the near-surface region was $\sim 1.0\times 10^{21}$. After converting this concentration to an atomic fraction, it can be seen from Fig. 10 that the calculated cell size is ~ 500 Å. The Ga results are somewhat more difficult to interpret because of the loss of dopant that occurs and because the Ga distribution is rather sharply peaked in the near-surface region (Fig. 11, Ref. 15). A concentration of 8×10^{20} seems not unreasonable and from Fig. 10 gives a cell size of ~ 1200 Å. Smaller cell sizes would undoubtedly be obtained if corrections for dopant loss could be made, or if the value of k_i from the VDAE model were somewhat smaller than that shown in Fig. 2. Trumbore has reported a value of $k_i^0 = 8\times 10^{-6}$ for Fe in Si but no values of D_l for Fe in liquid Si are available. As discussed in Sec. III C, a value of $D_l = 8\times 10^{-4}$ cm^2/sec was chosen for Cu, Au, Ag, Co, and Fe when calculating $k_i = k_i(v)$. An estimate of the concentration of Fe in the samples examined by Narayan is not available to the author, but Fig. 10 shows clearly that the calculated cell size for Fe follows the observed trend quite well.

After this paper was virtually completed, a brief account of experiments and calculations on cellular formation of In in Si during pulsed-laser annealing was published by Cullis *et al.*[37] It appears that there may be some fundamental differences between the experimental results in Ref. 15 and 37 and between the calculations reported here and in Ref. 37. For example, the data in Table I given by Cullis *et al.* seem to imply that under experimental conditions not greatly different from those used in Ref. 15, approximately 1.1 atomic percent of In can be put into Si substitutionally at a recrystallization velocity of 4 m/sec. White *et al.* found that only $\sim 0.3-0.4$ atomic percent of In could be incorporated into Si at a melt-front velocity of $4-4.5$ m/sec. If this interpretation of the Cullis *et al.* data is correct, the calculations in this paper give results which fall in between the results of Ref. 15 and 37. However, without more detailed information about the work of Cullis *et al.*, it is difficult to make a meaningful comparison of their results, the results reported in Ref. 15, and the calculated results reported here.

VI. DISCUSSION

The reader will have realized that numerous simplifying assumptions have been made in arriving at the VDAE model and the results described in the preceding sections. Many of these assumptions are typical of those often made in traditional theories of solidification processes in binary systems, e.g., ideal dilute solutions, and the success of these theories argues for the basic validity of these assumptions. The fact that the assumptions also apparently work well in the present model indicates that the ultrarapid solidification, as such, does not alter their validity. It is really rather remarkable that the introduction of the concept of velocity-dependent activation energies within the framework of a simple kinetic rate model leads to such satisfying explanations of so many of the observed results. On the other hand, it is almost intuitively clear that the activation energy for a transition of a dopant atom from the solid to the liquid must depend on the velocity of the liquid-solid interface. The reader will also realize that on many of the figures the calculations have been extended beyond the apparent range of validity of the model; this was done primarily for illustrative purposes. A thorough testing of the model and its range of validity can only be made as more experimental data is accumulated and the model itself is further developed. In this section, therefore, rather than discuss in greater detail some of the finer points of the model, we will devote our attention to several areas of more general interest.

A. "Solute Trapping"

Baker and Cahn[9,38] have used the terminology "solute trapping" to describe the situation in which a solute atom experiences an *increase* in chemical potential as it crosses the interface. In this subsection it will be shown that the model developed here satisfies the Baker and Cahn criterion for solute trapping in dilute solutions.

Baker and Cahn have given the following example of the calculation of the change in chemical potential for a simple case in which dilute solutions are present in both the solid and liquid. For such solutions the chemical potentials of the dopant in the solid and liquid are given, respectively, by Henry's law:

$$\mu_d^s = B^s + RT\ln(\gamma^s C_d^s)\ , \tag{49a}$$

$$\mu_d^l = B^l + RT\ln(\gamma^l C_d^l)\ . \tag{49b}$$

The B's and γ's are related constants which depend on the temperature and reference state for the ener-

gy. The constants may be eliminated by using the condition that μ_d^s and μ_d^l must be equal at equilibrium, i.e., when $C_d^s = C_d^{s0}$ and $C_d^l = C_d^{l0}$; C_d^{s0} and C_d^{l0} are the concentrations in the solid and liquid at equilibrium. The change in the chemical potential experienced by a *single* dopant atom as it crosses the interface region is then given by

$$\Delta\mu_d = \mu_d^s - \mu_d^l = kT \ln\left[\frac{C_d^s}{C_d^{s0}}\frac{C_d^{l0}}{C_d^l}\right] \tag{50}$$

or, since $k_i^0 = C_d^{s0}/C_d^{l0}$ and $k_i = C_d^s/C_d^l$,

$$\Delta\mu_d = kT \ln(k_i/k_i^0) . \tag{51}$$

Since the B's and γ's are temperature dependent and were eliminated by using equilibrium conditions, the T in Eqs. (49a) and (49b) is the temperature appropriate for solidification under nearly equilibrium conditions. For dilute solutions, T is approximately T_h, the melting point of the pure material, and therefore

$$k_i = k_i^0 \exp(\Delta\mu_d/kT_h) . \tag{52}$$

Comparing this to Eq. (18), it is found that

$$\Delta\mu_d = -kT_h \ln k_i^0 f(v) . \tag{53}$$

At or very near equilibrium $v \simeq 0$, $f(v) \simeq 0$, and the dopant experiences no change in chemical potential as it crosses the interface. For very high interface velocities $f(v) \to 1$, and the maximum value of the change in chemical potential is ΔU_d^{ra} of Eq. (17). Thus, the model developed here does indeed imply an increase in the chemical potential if k_i is to exceed k_i^0, as Baker and Cahn require.

It is worthwhile to consider in more detail the relationship between the requirement for a positive value of $\Delta\mu_d$ for solute trapping to occur and the physical content of the model developed here. It is not sufficient to examine the energy diagrams of Fig. 5 because none of the quantities shown there are the chemical potentials which exist during the solidification process. As explained at the end of Sec. III D, the vibrational energies of the dopant atoms are not included in these diagrams. Let us go back to Eq. (11) and calculate k_i on the basis of the developments in Secs. III A, III B, and III D. From Eqs. (11), (12), (13), and (16) we have

$$k_i = (A_d^f/A_d^r)\exp\{-[U_d^f - U_d^{r0} - \Delta U_d^r(v)]/kT\} . \tag{54}$$

It has been previously assumed that $K_d^f = K_d^{f0}$ (Eq. 10) and that $A_d^f = A_d^{f0}$, and therefore it follows that $U_d^f = U_d^{f0}$. Assuming that $T \simeq T_h$ and using Eqs. (34), (36), and (37), it can be shown that

$$k_i = \exp\{[(U_d^s - U_d^{r0})f(v) - (U_d^s - U_d^{ro})]/kT_h\} , \tag{55}$$

which is nothing more than another form of Eq. (18). Equation (22) can be used to put k_i in the form

$$k_i = k_i^0 \exp[(U_d^s - U_d^{r0})f(v)/kT_h] . \tag{56}$$

What has been demonstrated by this exercise is that the quantities appearing on the energy-level diagrams can be used to get back to the expression for k_i. From Eqs. (54) and (55) it is seen that the quantity U_d^{r0} appears explicitly. In spite of this, it should be clear by now that U_d^{r0} cannot be determined from the model developed here, although the difference $U_d^s - U_d^{r0}$ can be. Since k_i^0 of Eq. (56) already contains the ratio of the A's given in Eq. (34), the quantity $(U_d^s - U_d^{r0})f(v)$ represents the true change in the chemical potentials. The velocity dependence of this quantity can be interpreted in the following manner. The thermodynamic considerations of Baker and Cahn[38] put the very general requirement on the system that if k_i is observed to be greater than k_i^0 there must have been an increase in the chemical potential of the dopant atoms as they crossed the interface. Nothing however is said about the physical mechanism by which this increase is obtained; the terminology "solute trapping" is defined only in terms of the increase in the chemical potential and solidification at near-equilibrium rates. Loosely speaking, the VDAE model developed here shows how the increase in chemical potential implied by the thermodynamic arguments is compensated by the velocity-dependent U_d^r so that solute trapping can actually occur. Thus, the build-up in U_d^r with velocity is always exactly enough to compensate the increase in $\Delta\mu_d$ implied by the ratio of k_i/k_i^0 that is obtained. However, it should be noted that since an upper limit to U_d^r is given by U_d^s, there may very well be some dopants for which U_d^r will not be sufficient to ensure complete trapping ($k_i = 1$) in a dispersed phase.

B. Limitations of a thermodynamic approach to pulsed-laser annealing

It has already been emphasized that the large departures of k_i from k_i^0 (Table I) and the fact

that the conventional solubility limits for some dopants can be exceeded by orders of magnitude show that the ultrarapid solidification characteristic of pulsed-laser annealing involves processes occurring well away from thermodynamic equilibrium. Since conventional phase diagrams always assume thermodynamic equilibrium to hold, it is legitimate to question the application of conventional thermodynamic concepts and the predictions of thermodynamics to the laser-annealing process. Specifically, thermodynamic approaches to the solidification problem invariably involve the requirement that the liquid-solid interface be at some temperature. This requirement is necessary in order to relate various quantities to the phase diagrams. Since, in principle, equilibrium thermodynamics does not even allow for the motion of the liquid-solid interface, it is necessary to introduce rate equations of the type appearing in Sec. III A in order to have a theory of solidification. For the freezing of a one-component liquid, simple considerations based on rate equations leads to the expression (Ref. 31)

$$v=\frac{L_h K_h^r}{RT_h^2}(T_h-T)\ . \tag{57}$$

In such an equation, T is usually referred to as the "temperature of the interface" or T_h-T is called the "degree of undercooling." This terminology may have some meaning when conventional freezing rates are being considered, but its meaning is more difficult to specify when applied to ultrarapid solidification phenomena.

The differential-equation approach to the solidification problem shows that it is the gradient of the temperature at the interface that determines the melt-front velocity [Eq. (45)]. The calculations of paper I, which were based on the finite-difference heat diffusion equation, in effect required the interface to be at the melting temperature of the material during the solidification process. Of course, as we have already seen in this paper, the interface should be thought of as having finite dimensions and not as a dividing plane between the solid and liquid. This again illustrates the difficulties involved in trying to define a quantity that could be called the "temperature of the interface". Moreover, even if such a concept had meaning it would be virtually impossible to measure the "interface temperature" during rapid solidification. Recognition of this difficulty led Baker and Cahn[9] to consider a retrograde system (Zn-Cd) for which it is not necessary to know the temperature of the interface in order to establish that deparatures from local thermodynamic equilibrium have occurred.

The foregoing discussion is not meant to imply that equilibrium thermodynamic data and phase diagrams are of no value in studying nonequilibrium phenomena. This is clearly not the case, as is illustrated by the MS treatment of cellular formation. Moreover, it seems possible to utilize Eq. (57) to set up a rough operational correspondence between the melt-front velocity and the temperature of the interface. However, the utility of this equation is limited by reliable information about the rate constant K_h^r. In any case, when large departures from equilibrium occur, as they evidently do during pulsed-laser annealing, predictions based on equilibrium thermodynamic concepts should be treated with caution. For this reason, it should not be surprising if "absolute" solubility limits[39] based on the thermodynamic considerations of Baker and Cahn[38] are exceeded at the high recrystallization velocities attained during pulsed-laser annealing.

C. Anisotropic segregation effects

Indications that k_i may be dependent on the *direction* of crystal growth have been in the literature[40] for some time. Under the nonequilibrium conditions of pulsed-laser annealing, directional effects are likely to become more apparent and it is of interest to consider their origin in terms of the VDAE model. Since k_i is dependent on the growth velocity through $U_d^r(v)$, if v were dependent on growth *direction,* there would be a directional dependence automatically imparted to k_i. It is possible that v does depend on growth direction during laser annealing, but it is unlikely that this dependence is strong. Moreover, the heat transport equations used in Ref. 1 do not provide a mechanism for direction-dependent solidification rates; therefore, a direction dependence for v will not be considered further here. Instead, it will be recognized that U_d^r most likely depends on direction through v_0 of Eqs. (19a) and (19b). In order to see how this can come about, the consequences of the layer structure which forms in the interface region[41] as the transition from the liquid to the solid state evolves will be considered in more detail.

Study of the Si lattice shows that in the [100] direction, the covalent bonding with a given Si atom, or with a comparably bonded group III or V dopant atom, involves three planes of atoms

separated by a total distance of $\Delta x(100)=a/2$, where a is the lattice constant. Δx will be called the repeat distance. The corresponding distances for the [111] and [110] directions are $\Delta x(111)=a/\sqrt{3}$ and $\Delta x(100)=a/\sqrt{2}$, respectively. The spacing δx between the planes is uniform in the [100] and [110] directions, but not in the [111] direction. Based on these simple considerations, it might be concluded that dopant atoms would be incorporated into the solid most efficiently in the [100] direction. However, such considerations do not take into account the strong tendency for dopant atoms to make transitions back toward the liquid (see Fig. 1). A model which by necessity must be greatly oversimplified, but which does take this tendency into account will now be sketched.

Suppose that during crystallization the atoms in an entire layer are deposited in a time interval $\delta t(hkl)=\delta x(hkl)/v$. Suppose further that the nth layer has just been completed during crystallization in the $[hkl]$ direction. While the nth layer was forming, the $n+1$ layer was also beginning to form (this is indicated schematically by the oscillations in region I of Figs. 1 and 5). Before the $n+1$ layer can be completed a dopant atom in the nth layer may make a jump into a vacancy in the $n+1$ layer. Let $P_i(hkl)$ be the probability per unit time that such a jump of the dopant atom occurs; the subscript i is necessary to distinguish the different interlayer spacings $\delta x_i(hkl)$ contained in $\Delta x(hkl)$; e.g., $i=2$ in the [111] direction. The velocity of a dopant atom in the interface region (Fig. 1), time averaged over the repeat distance, is given approximately by

$$v_0(hkl)=\sum_i P_i(hkl)\delta t_i(hkl) \times \delta x_i(hkl)/\Delta t(hkl) \qquad (58)$$

with $\Delta t(hkl)=\Delta x(hkl)/v$.

A rigorous calculation of $P_i(hkl)$ and hence $v_0(hkl)$ would be virtually impossible since it would involve the calculation of frequency factors, accommodation coefficients, activation energies, etc. for transitions in the interface region about which we have no detailed knowledge. In order to make any progress at all, it will be assumed that the $P_i(hkl)$ are simply proportional to the fractional number of unformed bonds associated with a dopant atom in the nth layer. For example, in the [100] direction an atom in the nth layer forms bonds with two atoms in the $n-1$ layer and can have two bonds with the $n+1$ layer which is forming; hence $P_1(100)\propto 1/2$. Similarly, for the [111] direction $P_1(111)\propto 1/4$ and $P_2(111)\propto 3/4$. The [110] direction presents a special problem because in a perfect crystal an atom in any (110) plane is bonded to two other atoms *in the same plane*. Thus, while the nth plane is forming, the number of bonds a dopant atom has with host atoms in the same plane changes from zero to two. There is no obvious way around this difficulty at the level of the approximations being made here and so it will be assumed that on the average during the time the nth plane is forming a dopant atom is bonded to one other atom in the plane; hence $P_1(110)\propto 1/2$.

When the details of the procedure given above are worked out and the various quantities are substituted into Eq. (58) it is found that $v_0(111)=0.866v_0(100)$ and $v_0(110)=1.414v_0(100)$. Figure 11 shows the results of calculations of $k_i(hkl)$ for Sb and Bi in Si using Eq. (19b) for $U_d'(v)$. Although these results have little more than qualitative significance,[42] in arriving at the value of $v_0(111)$ it became evident that the interplanar spacings and the bonding properties in the [111] direction are such that dopant atoms cannot move as readily in this direction as they can in the [100] and [110] directions. It should be noted that since $v_0(100)$ was related to D_i by $v_0=D_i/x_0$ and to D_l by $v_0=D_l/x_0'$ [see discussion following Eq. (20)], variations of v_0 are equivalent to variations of D_l with x_0' kept fixed. Thus, Fig. 11 also gives an indication of the sensitivity of k_i to uncertainties in the values of D_l.

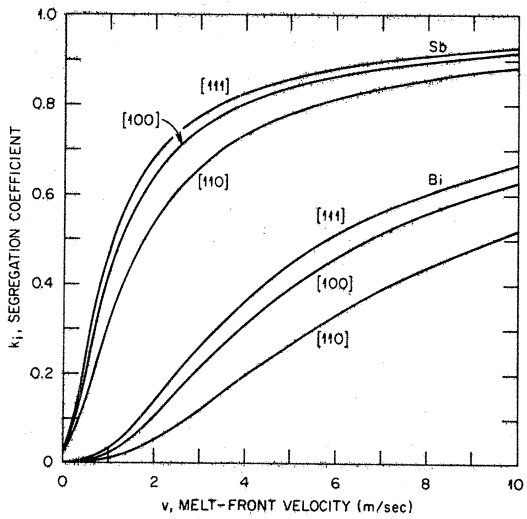

FIG. 11. Variation of k_i with velocity and with the direction of crystal growth obtained from the very simple model described in Sec. VI C.

D. Other models of nonequilibrium segregation

There have been a number of attempts in the past to describe the dependence of the interface segregation coefficient on the velocity of the liquid-solid interface. These attempts will be reviewed very briefly here and, where possible, related to the VDAE model.

Jackson[19] took an approach based on kinetic rate theory and came to the conclusion that the dependence of k_i on v was very weak. Baker and Cahn[9] subsequently pointed out that Jackson's theory did not satisfy the thermodynamic criterion for solute trapping and therefore could not be correct. The difference between Jackson's approach and the VDAE model is that Jackson did not allow the rate constants to depend explicitly on the interface velocity. The types of arguments that Jackson used to obtain a v-dependence of k_i are essentially the same as those used to derive the temperature dependence of k_i^0. As a result, his derivation was tied too closely to equilibrium phase diagrams, and could not apply to truly nonequilibrium segregation.

Thurmond[31] has given a simple expression for the dependence of k_i on v, also based on kinetic rate theory. In fact, his expression is essentially the same as Eq. (8) of this paper which, as we have seen, gives the wrong velocity dependence to k_i. Again, the reason for this incorrect behavior is the neglect of the velocity dependence of the rate constants themselves.

Baker and Cahn[38] have given critiques of four theories of solidification based on irreversible thermodynamics. Each theory is shown to have its shortcomings and the interested reader should consult Ref. 38 for the details. Here, however, it is of interest to discuss a few features of the Jindal-Tiller theory.[8] These authors divided the interface region into a number of layers each of which is regarded as an open thermodynamic system undergoing irreversible changes. While the layer nearest the solidified material is undergoing a phase transition, it is also exchanging atoms with the layer next to it, and so forth. In this respect, the Jindal-Tiller model resembles the VDAE model developed here. The major problem Jindal and Tiller encountered was the difficulty of solving the simultaneous equations for any number of layers greater than one. The VDAE model in some sense glosses over this problem by the time-averaging process leading to Eqs. (19a) and (19b). Jindal and Tiller obtained an expression for k_i which has the right behavior at large values of v but does not go to k_i^0 as v goes to zero.

At least two theories of nonequilibrium segregation based on modifications of the differential-equation approach to solidification theory have been proposed. As might be expected, the modifications involve the assumptions made about the interface region. Whereas the more standard derivations based on the diffusion equation treat the interface as a planar discontinuity (Ref. 11), the formulations of Chernov[43] and Baker[44] recognize that the interface region must have finite width and properties which are intermediate between those of the solid and liquid. In this respect, these two theories, are similar to one another and to the VDAE model. There appears to be enough flexibility built into the theories of Chernov and Baker to account in principle for the nonequilibrium effects involved in ultrarapid solidification. Cahn *et al.*[35] have illustrated the interface velocity dependence of k_i which follows from Baker's model when various assumptions about the interface region are made.

All of the models discussed above were formulated before the discovery of pulsed-laser annealing and at a time when little or no experimental data was available as an aid in the development of the models. In addition to the VDAE model, two other models have been proposed in response to the developments in the field of laser annealing.

Jackson *et al.*[45] have proposed a model which in some ways resembles the VDAE model described here; however, it seems to have some builtin inconsistencies. These authors simply add a term proportional to the velocity to the numerator of Eq. (8) (with $K_d = K_d^{f0}$ and $K_d^r = K_d^{r0}$), i.e.,

$$k_i = \frac{K_d^{f0} + \alpha v}{K_d^{r0} + v} . \tag{59}$$

The parameter α is interpreted as the fraction of dopant atoms in the layer adjacent to the interface which is trapped. Thus the maximum value α can have is one, which should lead to the maximum value of k_i. Jackson *et al.* claim that it is fairly unlikely that $k_i \simeq 1$ in alloys with retrograde solubility, but we have seen that $k_i \simeq 1$ for P, As, and Sb in Si. Moreover, Jackson *et al.* point out that the above equation predicts that k_i approaches α as v increases, which is certainly true. However, this implies that $v >> K_d^{r0}$ and $\alpha v >> K_d^{f0}$, which seems highly unlikely. Also, it should be noted

that by adding the term αv to the numerator of Eq. (59), Jackson *et al.* imply that the rate constant for a dopant atom jumping *into* the solid increases rapidly with velocity. To this author, it seems much more in accord with the concept of solute trapping to make the rate constant for jumps *out* of the solid the one that changes rapidly with velocity, as the VDAE model does.

Morehead[46] has described a finite difference calculation of dopant diffusion which incorporates kinetic rate effects at the interface. These calculations seem to incorporate a number of features which resemble aspects of the VDAE model. The values of the rate constants used by Morehead are substantially smaller than those used in this paper. Also, the agreement between experiment and his calculated values of the maximum concentration to be expected at any velocity is not good; the experimental and calculated values differ by more than an order of magnitude in many cases.

Finally, before leaving this discussion of other models and calculations, it is of interest to note that Hall,[40] as early as 1952, proposed an expression for k_i as a function of interface velocity which is based on concepts similar to those invoked later by many people (including the author) who have worked on the nonequilibrium segregation problem. Unfortunately, to this author's knowledge, Hall never published the details of the model and the equations on which his final expression for $k_i(v)$ was based.

VII. SUMMARY AND CONCLUDING REMARKS

In paper I of this series the heat transport equation, cast in finite difference form to allow for temperature-dependent thermal properties and melting, was solved for many different situations. From a series of these solutions for a given model, the position of the liquid-solid interface or melt front as a function of time was obtained. The duration of surface melting followed directly from these calculations. Also, the velocity of the melt front was calculated as a function of position and time. To a first approximation, it was found that the melt front velocity during solidification is constant, and that an average value could be extracted for use in other calculations.

In the second paper of the series, information about the melt front from paper I was used in calculations of dopant diffusion. Dopant diffusion coefficients in solid silicon are several orders-of-magnitude smaller than the corresponding values in the liquid and the experimental data show that only values of D_l can explain the spreading of the dopant profiles during pulsed-laser annealing of ion-implanted samples. Hence, knowledge of the time during which a given part of the sample is molten is crucial to the calculations. The experimental data show clearly that values of the interface segregation coefficients must be chosen much greater than the equilibrium values. In paper II, k_i was taken as an adjustable parameter without inquiring into the mechanism for nonequilibrium effects. The values of k_i differed from the equilibrium values by several orders of magnitude for some dopants.

In this third and final paper in the series, a model based on kinetic rate theory and using activation energies which depend on the melt-front velocity has been discussed in detail. This model gives the dependence of k_i on v in terms of a function $f(v)$ whose limiting behavior at small and large values of v can be prescribed, but whose exact form would be extremely difficult to calculate. Simple analytical forms of $f(v)$ which give good agreement with the limited amount of experimental data now available were introduced. Using approximations for dilute alloys frequently found in the literature, an expression for the concentration of a dopant in the solid as a function of v was obtained, and found to give reasonably good agreement with experimental results. Next, it was shown that when the expressions for $k_i = k_i(v)$ are used in the Mullins and Sekerka theory of cellular formation satisfactory agreement with experiment is obtained. If, on the other hand, the equilibrium value of $k_i = k_i^0$ is used there is no agreement whatsoever with experiment. It was shown that the model introduced in Ref. 3 and developed here satisfies the Baker and Cahn criteria for solute trapping, i.e., that the change in the chemical potential of a dopant atom in going from the liquid to the solid is positive for values of k_i greater than k_i^0. It was pointed out that the traditional thermodynamic approach of assigning a temperature to the interface region may need modifications when the temperature gradients are very large, as they are in pulsed-laser annealing. The dependence of k_i on the direction of crystal growth was discussed on the basis of a very simple model. Finally, attempts of other authors to obtain expressions for the velocity dependence of k_i were reviewed and compared to the VDAE model developed here.

Although some authors continue to dispute the validity of the melting model of pulsed-laser annealing,[47,48] it seems to this author that the remarkable agreement between theory and experiment obtained with this model argues almost overwhelmingly for its essential validity. In any case, it is difficult to exaggerate the importance of the laser-annealing phenomena. From the standpoint of basic solid-state physics and materials science, it has provided for the first time a method for achieving ultrarapid recrystallization under well-controlled conditions. It thus opens up possibilities for exploring nonequilibrium thermodynamic effects that were not previously accessible to experimentation. From a more applied viewpoint, pulsed-laser annealing offers a variety of new fabrication techniques for semiconductor devices. Many of these techniques have already been applied to the fabrication of high-efficiency single-crystal silicon solar cells[49,50] and laser-induced melting shows promise of being a useful tool in the study of grain boundary effects in polycrystalline materials.[51] The metastable alloys formed when the equilibrium solubility limit is surpassed during pulsed-laser annealing are essentially new materials whose properties and applications are just beginning to be extensively investigated. It is not difficult to understand why laser annealing, or more generally laser processing, has generated such intense interest among solid-state physicists and materials scientists.

ACKNOWLEDGMENTS

I am particularly grateful to F. W. Young, Jr. for numerous useful discussions, for critical readings of several versions of the manuscript, and for general interest in the progress of the work reported here. This research was sponsored by the Division of Materials Sciences, U. S. Department of Energy under Contract No. W-7405-eng-26 with the Union Carbide Corporation.

---

[1]R. F. Wood and G. E. Giles, Phys. Rev. B 23, 2923 (1981).
[2]R. F. Wood, J. R. Kirkpatrick, and G. E. Giles, Phys. Rev. B 23, 5555 (1981).
[3]R. F. Wood, Appl. Phys. Lett. 37, 302 (1980); R. F. Wood, J. C. Wang, G. E. Giles, and J. R. Kirkpatrick, in *Laser and Electron Beam Processing of Materials*, edited by C. W. White and P. S. Peercy (Academic, New York, 1980), p. 37.
[4]W. W. Mullins and R. F. Sekerka, J. Appl. Phys. 35, 444 (1964).
[5]I. B. Khaibullin, E. I. Shtyrkov, M. M. Zaripov, M. R. Galyautdinov, and G. G. Zakirov, Fiz. Tekh. Poluprovodn. 11, 330 (1977) [Sov. Phys.—Semicond. 11, 190 (1977)].
[6]J. C. Wang, R. F. Wood, and P. P. Pronko, Appl. Phys. Lett. 33, 455 (1978).
[7]P. Baeri, S. U. Campisano, G. Foti, and E. Rimini, Appl. Phys. Lett. 33, 137 (1978); J. Appl. Phys. 50, 788 (1979).
[8]B. K. Jindal and W. A. Tiller, J. Chem. Phys. 49, 4632 (1968).
[9]J. C. Baker and J. W. Cahn, Acta Metall. 17, 575 (1969).
[10]F. A. Trumbore, Bell Syst. Tech. J. 39, 205 (1960).
[11]See, for example, V. G. Smith, W. A. Tiller, and J. W. Rutter, Can. J. Phys. 33, 723 (1955) and the brief review in Ref. 2 above.
[12]C. W. White, J. Narayan, and R. T. Young, Science 204, 461 (1979).
[13]R. T. Young, J. Narayan, and R. F. Wood, Appl. Phys. Lett. 35, 447 (1979).
[14]K. A. Jackson and H. J. Leamy, in *Laser-Solid Interactions and Laser Processing*, edited by H. J. Leamy and J. M. Poate (American Institute of Physics, New York, 1979), p. 102.
[15]C. W. White, S. R. Wilson, B. R. Appleton, and F. W. Young, Jr., J. Appl. Phys. 51, 738 (1980).
[16]J. R. Poate, H. J. Leamy, T. T. Sheng, and G. K. Celler, Appl. Phys. Lett. 33, 918 (1978); G. J. van Gurp, G. E. Eggermont, Y. Tamminga, W. T. Stacy, and J. R. M. Gijsbers, Appl. Phys. Lett. 35, 273 (1979).
[17]A. G. Cullis, J. M. Poate, and G. K. Celler, in *Laser-Solid Interactions and Laser Processing*, Ref. 14, p. 311; J. Narayan, J. Met. 32, 15 (1980).
[18]I would like to thank F. W. Young for first bringing this to my attention.
[19]K. A. Jackson, Can. J. Phys. 26, 683 (1958).
[20]B. Chalmers, Trans. AIME 200, 519 (1954).
[21]H. Kodera, Jpn. J. Appl. Phys. 2, 212 (1963).
[22]Y. M. Shashkov and V. M. Gurevich, Zh. Fiz. Khim. 42, 2058 (1968) [Russ. J. Phys. Chem. 42, 1082 (1968)].

[23]C. W. White, B. R. Appleton, B. Stritzker, D. M. Zehner, and S. R. Wilson, in *Laser and Electron-Beam Solid Interactions and Materials Processing,* edited by J. F. Gibbons, L. D. Hess, and T. W. Sigmon (Elsevier North-Holland, Amsterdam, 1981), p. 59.

[24]A. G. Cullis, H. C. Webber, J. M. Poate, and A. L. Simons, Appl. Phys. Lett. 36, 320 (1980); R. F. Wood and G. E. Giles, *ibid.* 38, 422 (1981).

[25]F. Seitz, in *The Modern Theory of Solids* (McGraw-Hill, New York, 1940), p. 345.

[26]C. Kittel, in *Introduction to Solid State Physics,* 4th ed. (Wiley, New York, 1971), p. 95.

[27]See, for example, L. Pauling, in *Nature of the Chemical Bond,* second edition (Cornell University Press, Ithaca, 1948); also W. A. Harrison, in *Electronic Structure and the Properties of Solids* (Freeman, San Francisco, 1980), p. 167.

[28]K. Weiser, J. Phys. Chem. Solids 7, 118 (1958).

[29]T. L. Allen, J. Chem. Phys. 27, 810 (1957).

[30]See B. L. Sharma, *Diffusion in Semiconductors,* (Trans. Tech., Clausthal-Zellerfeld, Germany, 1970), and references therein.

[31]See, for example, C. D. Thurmond, in *Semiconductors,* edited by H. B. Hannay (Reinhold, New York, 1959), p. 145.

[32]D. R. Stull and G. C. Sinke, *Thermodynamic Properties of the Elements,* No. 18 in Advances in Chemistry Series (American Chemical Society, New York, 1956).

[33]Micrographs showing cellular structure in various materials solidified under a variety of conditions appear in the article by L. A. Tarshis, J. L. Walker, and J. W. Rutter, in *Metallography, Structures and Phase Diagrams,* Metals Handbook 8 (American Society for Metals, Ohio, 1973), p. 150.

[34]W. A. Tiller, K. A. Jackson, J. W. Rutter, and B. Chalmers, Acta Metall. 1, 428 (1953).

[35]J. W. Cahn, S. R. Coriell, and W. J. Boettinger, in *Laser and Electron Beam Processing of Materials,* Ref. 3, p. 89.

[36]J. Narayan, J. Appl. Phys. 52, 1289 (1981).

[37]A. G. Cullis, D. T. J. Hurle, H. C. Webber, N. G. Chaw, J. M. Poate, P. Baeri, and G. Foti, Appl. Phys. Lett. 38, 642 (1981).

[38]J. C. Baker and J. W. Cahn, *Solidification* (American Society for Metals, Metals Park, Ohio, 1971), p. 23.

[39]A discussion of these limits is given in Ref. 35.

[40]See, for example, R. N. Hall, Phys. Rev. 88, 139 (1952).

[41]It is interesting to note that molecular dynamics calculations of the properties of a liquid phase in contact with crystal phase shows layered structure in the interface region. See S. Toxvaerd and E. Praestgaard, J. Chem. Phys. 67, 5291 (1977).

[42]In a paper which appeared after this manuscript was completed, Baeri *et al.* report that k_i (111) is indeed greater than k_i (100) for a given melt-front velocity. See P. Baeri, G. Foti, J. M. Poate, S. U. Campisano, and A. G. Cullis, Appl. Phys. Lett. 36, 800 (1981).

[43]A. A. Chernov, *Growth of Crystals* (Consultants Bureau, 1962), Vol. 3, p. 35.

[44]J. C. Baker, Ph.D thesis, MIT, 1970 (unpublished), Chap. V. A brief description of Baker's model is given in Ref. 35 of this paper.

[45]K. A. Jackson, G. H. Gilmer, and H. J. Leamy, in *Laser and Electron Beam Processing of Materials,* Ref. 3, p. 104.

[46]F. Morehead, in *Laser and Electron Beam Processing of Materials,* Ref. 3, p. 143.

[47]H. W. Lo and A. Compaan, Phys. Rev. Lett. 44, 1604 (1980).

[48]J. A. van Vechten, in *Laser and Electron Beam Processing of Materials,* Ref. 3, p. 53.

[49]R. T. Young, R. F. Wood, J. Narayan, C. W. White, and W. H. Christie, IEEE Trans. Electron Devices ED-27, 807 (1980); R. T. Young and R. F. Wood, J. Appl. Phys. (in press).

[50]J. C. Muller, E. Fogarassy, D. Salles, R. Stuck, and P. M. Siffert, IEEE Trans. Electron Devices ED-27, 815 (1980).

[51]R. F. Wood, R. T. Young, R. D. Westbrook, J. Narayan, W. H. Christie, and J. W. Cleland, Sol. Cells 1, 381 (1980), Elsevier Sequoia Journal.